1    A New Instrument for Time Resolved Measurement of $HO_2$ Radicals

2    Thomas H. Speak[1], Mark A. Blitz[1,2]*, Daniel Stone[1] and Paul W. Seakins[1,2]*

3    *1 – School of Chemistry, University of Leeds, Leeds, LS2 9JT, UK*

4    *2 – National Centre for Atmospheric Science, Leeds, LS2 9JT, UK*

5    *Abstract*

6    OH and $HO_2$ radicals are closely coupled in the atmospheric oxidation and combustion of volatile
7    organic compounds (VOCs). Simultaneous measurement of $HO_2$ yields and OH kinetics can
8    provide the ability to assign site specific rate coefficients that are important for understanding the
9    oxidation mechanisms of VOCs. By coupling a FAGE LIF detection system for OH and $HO_2$ with
10   a high pressure laser flash photolysis system, it is possible to accurately measure OH pseudo-first-
11   order loss processes up to ~100000 $s^{-1}$ and to determine $HO_2$ yields via time resolved
12   measurements. This time resolution allows discrimination between primary $HO_2$ from the target
13   reaction and secondary production from side reactions. The apparatus was characterized by
14   measuring yields from the reactions of OH with $H_2O_2$ (1:1 link between OH and $HO_2$), with
15   $C_2H_4/O_2$ (where secondary chemistry can generate $HO_2$), with $C_2H_6/O_2$ (where there should be
16   zero $HO_2$ yield) and with $CH_3OH/O_2$ (where there is a well-defined $HO_2$ yield).

17   As an application of the new instrument, the reaction of OH with n-butanol has been studied at
18   293 and 616 K. The bimolecular rate coefficient at 293 K, $(9.24 \pm 0.21) \times 10^{-12}$ $cm^3$ molecule$^{-1}$ s$^{-1}$,
19   is in good agreement with recent literature, verifying that this instrument can measure accurate OH
20   kinetics. At 616 K the regeneration of OH in the absence of $O_2$, from the decomposition of the β-
21   hydroxy radical, was observed, which allowed the determination of the fraction of OH reacting at
22   the β site $(0.23 \pm 0.04)$. Direct observation of the $HO_2$ product in the presence of oxygen has
23   allowed the assignment of the α-branching fractions $(0.57 \pm 0.06)$ at 293 K and $(0.54 \pm 0.04)$ at
24   616 K), again in good agreement with recent literature; branching ratios are key to modelling the
25   ignition delay times of this potential 'drop-in' biofuel.

## 27 **1 Introduction**

28   In the atmosphere, $HO_2$ and OH radicals (OH + $HO_2$ = HOx) are closely coupled via several

29   reactions as shown in Scheme 1. The short lifetimes of HOx radicals mean that concentrations are

30   determined by chemical production and removal and not by transport processes, making them ideal

31   candidates as test species for our understanding of atmospheric chemical mechanisms (Stone et

32   al., 2012;Monks, 2005;Stockwell et al., 2012).

33
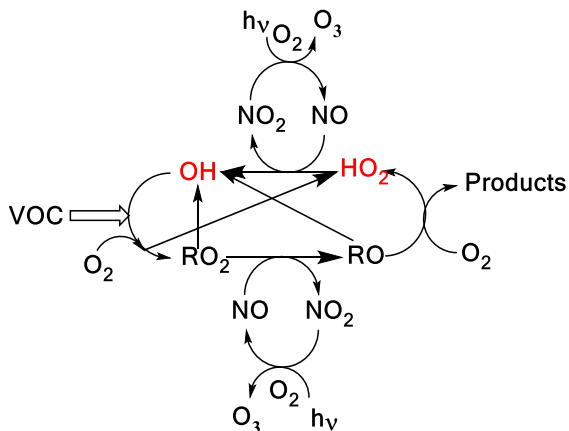
**Scheme 1.** A simplified tropospheric HOx cycle showing the importance of these short-lived radical species both to the chemical removal of VOCs and the formation of ozone.

36

In Scheme 1, the reaction of alkoxy radicals with molecular oxygen is a major route to $HO_2$ formation; however, this is not the only significant $HO_2$ formation process; for example, in the atmospheric oxidation of n-butanol, $HO_2$ can be formed via two different mechanisms. Abstraction by OH at the $\alpha$ position leads to a radical which reacts with oxygen to directly produce $HO_2$ (R1a, R2) whereas abstraction at other sites leads to alkylperoxy radical ($C_4H_9O_2$) formation with varying fractions of the $RO_2$ forming alkoxy radicals, and subsequently $HO_2$ (McGillen et al., 2013) on a longer timescale, see Scheme 2.

$$OH + CH_3CH_2CH_2CH_2OH \rightarrow CH_3CH_2CH_2CHOH + H_2O \qquad (R1a)$$

$$CH_3CH_2CH_2CHOH + O_2 \rightarrow HO_2 + CH_3CH_2CH_2CHO \qquad (R2)$$

The fraction of alkoxy radicals formed depends on the mechanism of $RO_2$ removal (reaction with NO or self or cross-reactions) and the yield of $HO_2$ from the alkoxy radical depends on the competition between decomposition, isomerization and reaction with $O_2$, which in turn will depend on the structure of the alkoxy radical, temperature, pressure and concentration of oxygen (Orlando et al., 2003). Therefore, in order to determine the $HO_2$ yield from the OH initiated oxidation of compounds such as n-butanol, it is important to have a selective, sensitive and time resolved method of $HO_2$ detection.
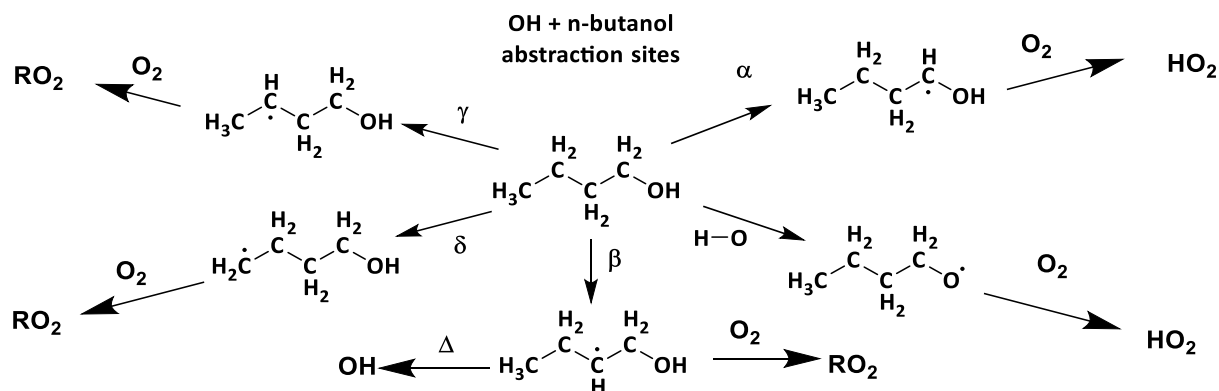
**Scheme 2.** The potential sites for OH abstractions in the oxidation of n-butanol. Of particular importance to low temperature combustion is the ratio of α to β branching fractions where α attack leads to chain inhibition and beta to chain propagation.

The importance of $HO_2$ chemistry is not limited to atmospheric processes; $HO_2$ is a key intermediate in low temperature (500 – 1000 K) combustion processes, particularly those involving oxygenated fuels (Zador et al., 2011). The mechanisms of low temperature combustion are of particular interest in the development of new engine technologies such as reactively controlled compression ignition (RCCI) (Reitz and Duraisamy, 2015) and are closely linked to atmospheric oxidation mechanisms. Monitoring $HO_2$ concentrations under the elevated temperatures and high pressures of combustion processes is therefore also of interest. In low-temperature combustion, $HO_2$ formation is a chain inhibition process, with OH reformation a chain propagating or chain branching process. The ratio of chain branching to chain inhibition processes is often the controlling factor in modelling ignition delay times (Agbro et al., 2017). High temperatures and concentrations of oxygen may be required to convert atmospheric processes, which take several 10s of seconds at ambient temperatures (and hence may be influenced by surface chemistry or secondary reactions) to the milli- or microsecond timescale where they can be studied by flash photolysis techniques without such interferences (Medeiros et al., 2018).

Direct measurements of $HO_2$ rely on absorption techniques, and kinetic information on $HO_2$ reactions has been determined mainly using absorption spectroscopy. This can be achieved either with conventional absorption techniques, often in the UV, (including multipass optics to enhance the pathlength) or in the IR with cavity ring down spectroscopy (CRDS) (Assaf et al., 2018;Onel et al., 2017). However, the $HO_2$ UV absorption spectrum (200 - 260 nm) is broad and

featureless (Crowley et al., 1991), and as such, overlaps with the UV absorptions of many other species present in atmospheric degradation pathways or combustion systems (particularly $H_2O_2$ and $RO_2$). To utilize the selectivity of the structured IR spectra, absorption methods have been developed in both the mid and near-IR (NIR) (Taatjes and Oh, 1997). Mid-IR absorption features for $HO_2$ provide sufficient absorption cross-sections for study (Jemialade and Thrush, 1990) but suffer from severe pressure broadening, reducing sensitivity under the conditions relevant to atmospheric and combustion systems (Thiebaud and Fittschen, 2006). Detection in the NIR has similar advantages in terms of a structured spectrum providing greater selectivity; the weaker absorption cross-sections are compensated by the higher powers and ease of use of NIR laser sources (Gianella et al., 2016). However, pressure broadening and interference from $H_2O$ absorptions can make these measurements difficult at even low concentrations of water ($10^{14}$ molecule $cm^{-3}$).

In the atmosphere (Stone et al., 2012) and in chamber studies (Glowacki et al., 2007), $HO_2$ is detected using a sensitive, but indirect method via conversion to OH, with detection of OH via laser induced fluorescence (LIF) (Hard et al., 1984;Brune et al., 1995;Fuchs et al., 2011) or conversion to $H_2^{34}SO_4$ with subsequent detection of the acid via mass spectrometry (Edwards et al., 2003;Hanke et al., 2002). In the LIF method, also known as Fluorescence Assay by Gaseous Expansion (FAGE (Hard et al., 1984)), which is the technique used in this study, OH is sampled into a low pressure region through a pinhole. Low pressures allow for the temporal separation of resonant 308 nm fluorescence from the excitation pulse. Following the first detection axis for OH, a flow of NO is introduced which reacts with $HO_2$ (R3):

$$HO_2 + NO \rightarrow OH + NO_2 \tag{R3}$$

The resulting OH is monitored at a second detector. The high sensitivity with which OH can be detected gives $HO_2$ detection limits in the $10^8$ molecule $cm^{-3}$ range for $5 - 10$ s averaging, however, to extract concentrations, both OH detection methods require calibration (Winiberg et al., 2015). For chamber measurements of $HO_2$, comparisons with direct CRDS measurements have verified the reliability of the calibration process (Onel et al., 2017).

$HO_2$ detection by LIF can be potentially sensitive to interferences from certain $RO_2$ species which may also be converted to OH on short timescales. Interferences can be minimized by short conversion times between NO injection and OH monitoring, utilizing low pressures, high flow

107    rates of the sample gas, and low NO concentrations to separate OH generation from $HO_2$ and $RO_2$,
108    reduced conversion of $HO_2$ reduces the sensitivity of this technique and as such in practice a
109    compromise between selectivity and sensitivity is used (Fuchs et al., 2011;Hard et al.,
110    1984;Whalley et al., 2013).

111        The current paper describes a significant development on our earlier FAGE based
112    instrument for time-resolved OH detection (Stone et al., 2016). In this improved system, laser flash
113    photolysis in a high pressure (up to 5 bar), temperature controllable (300 – 800 K) reactor (shown
114    in Figure 1) generated radicals which were then sampled through a pinhole forming a jet within
115    the low pressure detection region (shown in more detail in Figure 2). OH radicals were monitored
116    by LIF close to the pinhole. The jet breaks down after ~20 mm and NO was injected after this
117    point to convert some $HO_2$ into OH which was then detected by a second monitoring system. In
118    general, LIF becomes less sensitive at higher temperatures (due to distribution of population over
119    more rotational levels) and $O_2$ concentrations (due to quenching). Sampling into the low-pressure
120    region reduces both the effect of collisional quenching and temperature on the sensitivity of LIF
121    detection, although there is a reduction in the number density of the HOx species in the expansion.
122    We report the adaptation of our time-resolved OH-FAGE instrument to allow $HO_2$ detection, the
123    characterization of the instrument (including development of a calibration method for $HO_2$ yields
124    of OH initiated reactions), and the investigation of the influence of $RO_2$ species. Finally, we discuss
125    the application of the technique to determine the yield of $HO_2$ from the reaction of OH with n-
126    butanol. The instrument has some similarities to that presented by Nehr et al. (2011) where a
127    conventional OH lifetime instrument was altered to allow for chemical conversion of $HO_2$ to OH
128    and hence the sequential determination of OH and $HO_2$.

129

## 2 Experimental

131    Reactions were carried out in a high pressure (0.5 – 5 bar) reaction cell which is described in
132    greater detail in Stone et al. (2016) and schematics of which are shown in Figures 1 and 2. The
133    high-pressure reactor was a 0.5 m stainless steel tube with a 22 mm internal diameter. Gas flows
134    were delivered to the high-pressure cell from a mixing manifold where calibrated mass flow
135    controllers (MFC) allowed for accurate control of flow rates. Low vapour pressure compounds:
136    OH precursors ($H_2O_2$), and substrates methanol and butanol, were delivered to the mixing manifold

137  from, thermostatted bubblers in pressure regulated backing flows of nitrogen ($N_2$). Ethane and

138  oxygen were delivered directly from cylinders into the mixing manifold through MFCs. The gas

139  flowrate through the cell was kept under laminar conditions with typical Reynolds values (Re) of

140  480 (corresponding to a flow rate for an experiment of 10 SLM at 2 bar); in general conditions

141  were maintained between 400-800 Re   (Re < 2400 = laminar flow), with some experiments carried

142  out with higher flowrates, up to 1800 Re.

143      Temperature control of the reactor between room temperature and 800 K was achieved by

144  altering the voltage applied to a coil heater (WATROD tubular heater, Watlow) over the last 30

145  cm of the stainless-steel tube. The heated region was fitted with a quartz liner (inner diameter 18

146  mm) to reduce wall-initiated chemistry. A temperature readout, from a type K thermocouple in the

147  gas flow, close to the pinhole, was calibrated for given flow rates, pressures and voltage settings

148  by measuring the highly temperature sensitive OH and methane rate coefficient, using the

149  temperature dependence reported by (Dunlop and Tully, 1993).  A more detailed description of

150  this method is described within instrument characterization (Section 3.4).
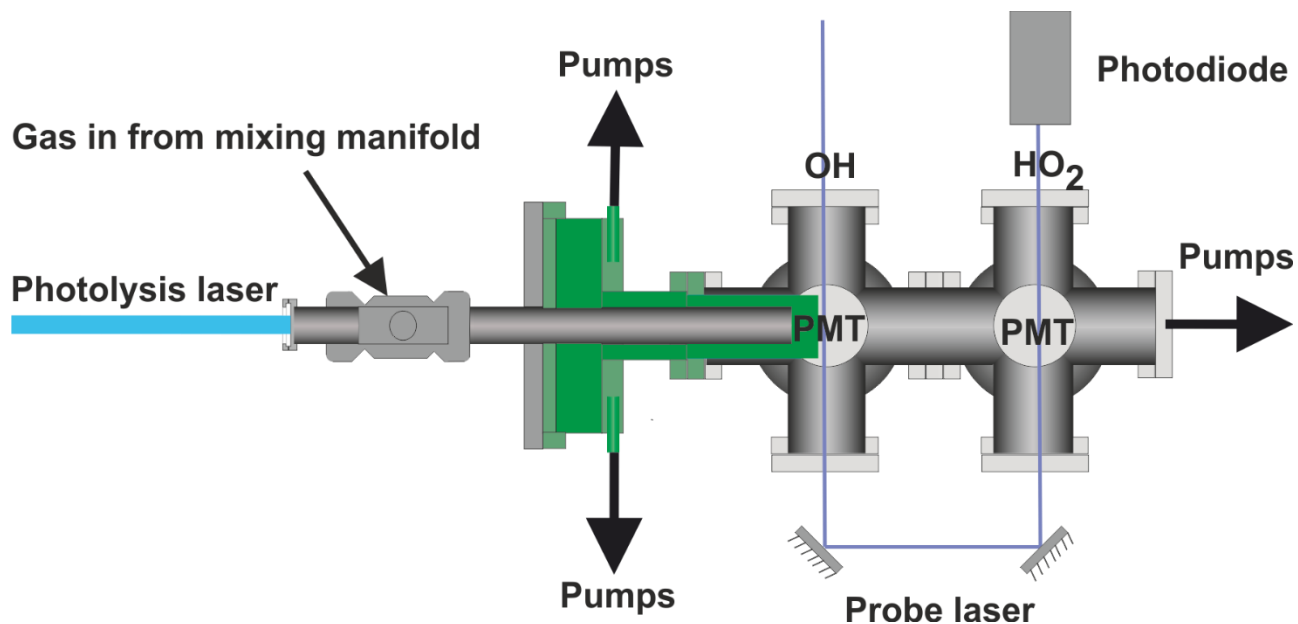
151

152  **Figure 1.** Schematic plan of the apparatus.

153

154      The photolysis of the OH precursor, $H_2O_2$, at 248 nm (Lambda Physik, Compex 200

155  operated using KrF at 1 or 5 Hz) or 266 nm (frequency quadrupled Nd-YAG output, Quantel, Q-

156    smart 850 at 1 or 10 Hz) initiated the chemistry. No significant difference was noted in the kinetics

157    or yields as a function of laser repetition rate.

158    $H_2O_2 + h\nu \rightarrow 2OH$                                                                                    (R4)

159    Hydrogen peroxide was used as the OH precursor for all experiments where $HO_2$ detection was

160    performed, because it also acts as an internal calibrant to relate OH and $HO_2$, via reaction R5:

161    **OH** $+ H_2O_2 \rightarrow H_2O +$ **$HO_2$**                                                                (R5)

162    However, in general, other OH precursors can be used. The OH precursor was maintained at low

163    concentrations ($1 \times 10^{14} - 1 \times 10^{15}$ molecule $cm^{-3}$) to minimise errors associated with assigning

164    pseudo-first-order kinetics for the loss of OH, and to reduce radical-radical reactions. Maintaining

165    a low radical precursor concentration had the additional advantage of minimising attenuation of

166    the photolysis beam, ensuring consistency in the initial radical concentrations generated along the

167    length of the high-pressure cell. Initial OH concentrations were in the range $2 \times 10^{11} - 5 \times 10^{13}$

168    molecule $cm^{-3}$.

169         A pinhole (diameter < 0.15 mm) at the end of the high-pressure reactor couples the reactor

170    to the low-pressure (0.3 – 5 Torr) detection cell. Details on OH detection can be found in Stone et

171    al. (2016). The accuracy of the instrument for OH measurement has recently been verified by

172    measurements of the rate coefficient of the reaction of OH with isoprene (Medeiros et al., 2018)

173    which are in excellent agreement with the literature. A more detailed schematic for the low-

174    pressure detection cell is shown in Figure 2.

175         In the first low pressure detection cell, the OH was probed within the jet expanded gas,

176    close to pinhole (<5 mm), perpendicular to the gas flow. The OH was detected by off-resonance

177    laser induced fluorescence (LIF) at 308 nm following excitation with 282 nm light ($A^2\Sigma$ ($v' = 1$)

178    $\leftarrow X^2\Pi(v'' = 0)$,$Q_{11}$). The 282 nm light was the frequency doubled output of a dye laser

179    ((Rhodamine 6 G, Spectron) pumped at 532 nm by a Nd:YAG laser (Spectron), or (Rhodamine 6

180    G, Continuum) pumped by a Nd-YAG laser (Quantel, Q-smart 850)). Measuring the off-resonance

181    fluorescence allowed the use of a filter ($308 \pm 5$ nm, Barr Associates) before the photomultiplier

182    (Perkin-Elmer C1943P) to remove scattered light and improved the signal to noise ratio.
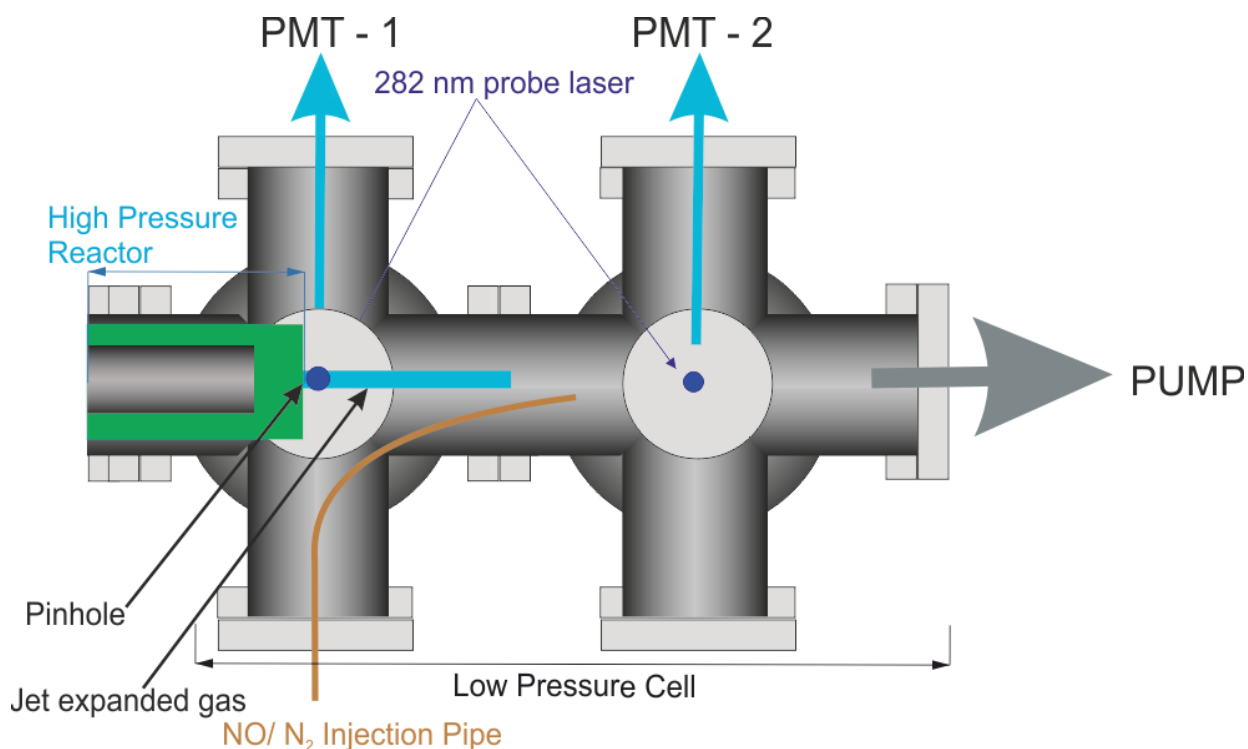
**Figure 2.** Detailed schematic elevation of the low-pressure detection region of the reactor. The blue line represents the jet expanded gas; the jet breaks down after approximately 2 cm. NO was injected through a 1.5 mm id stainless steel tube after the breakdown of the jet.

A delay generator (BNC DG535) was used to vary the delay (time resolution ~10 ns) between the photolysis and probe laser, facilitating generation of time profiles of the OH concentration. The traces, typically 200 – 300 data points and ranging in time from ~50 μs – 20 ms, were scanned through multiple times (5 – 20) and the signal at each time point was averaged, giving high precision OH loss traces. An example OH trace from the first detection cell for reaction R5 is presented in Figure 3. As reactions were carried out under pseudo first order conditions ([OH] << [substrate]), the time dependence of the OH LIF signal, $I_f$, (proportional to the [OH]) was given by:

$$I_{f,t} = I_{f,0}e^{-k_{OH}t}$$

where $k_{OH} = k_5[H_2O_2]$. In Figure 3 two traces are presented from the first, OH, detection axis, these two traces were taken in consecutive experiments with a constant $[H_2O_2]$ where the first trace ($k_{OH,1st} = (2351 \pm 22)$ s$^{-1}$) was taken where $N_2$ was flowed into the low pressure region, the second

200 trace ($k_{OH,1st} = (2389 \pm 18)$ s$^{-1}$) was taken when this flow had been switched to NO to allow HO$_2$

201 detection in the second detection cell, errors are given as 2 σ. The similarity of the OH decay traces

202 when either N$_2$ or NO was injected shows that there was no back streaming of NO in the low-

203 pressure cell and hence no HO$_2$ conversion at the first detection axis.
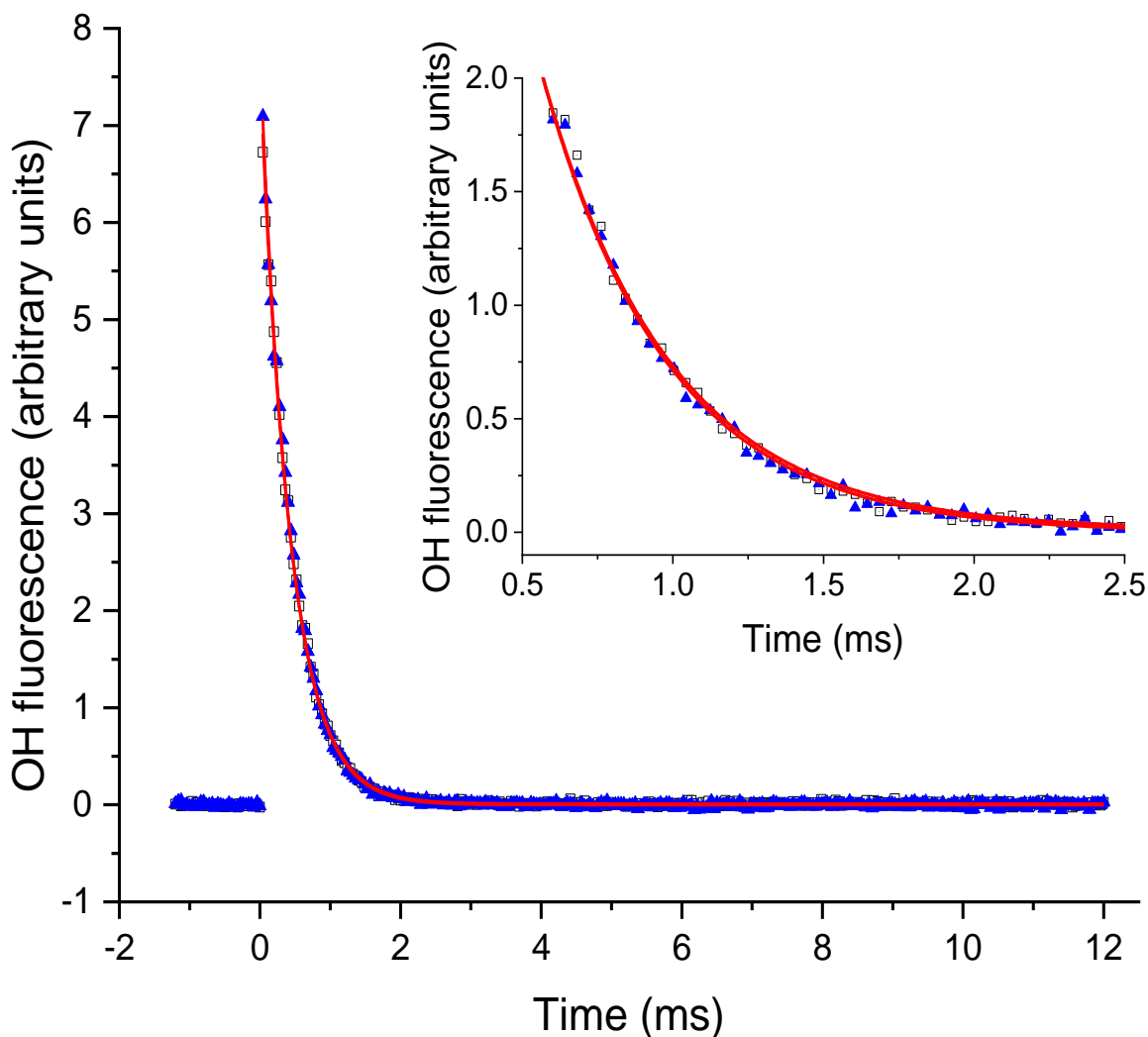
204

205 **Figure 3.** An example of the OH signal (solid blue triangles) collected at the first detection axis

206 for the reaction of OH with H$_2$O$_2$ ([H$_2$O$_2$] ≈ 1.4 × 10$^{15}$ molecule cm$^{-3}$, with a flow of N$_2$ into the

207 low-pressure cell, with open black squares representing the subsequent trace taken with a flow of

208 NO. The red lines represent the non-linear least squares fits to an exponential decay ($k_{OH,1st} =$

209 (2351± 22) s$^{-1}$ and $k_{OH,1st} = (2389 \pm 18)$ s$^{-1}$), 2 σ errors.

210

211        HO$_2$ radicals were monitored by the chemical transformation of HO$_2$ to OH via reaction

212    with NO (R3) in the low-pressure cell. Following the breakdown of the jet, after the Mach disk

213    (>2 cm beyond the pinhole), a small flow (5 sccm) of NO or N$_2$ was introduced into the low-

214    pressure cell via a 1.5 mm i.d. stainless steel pipe (for a typical 0.5 Torr pressure in the FAGE cell

215    the NO concentration was $5.5 \times 10^{13}$ molecule cm$^{-3}$). After passing through the first detection cell,

216    the probe beam was redirected through the second low-pressure detection cell downstream of the

217    NO pipe allowing for the measurement of the OH concentration by LIF in the same manner as in

218    the first cell.

219        By switching between a flow of N$_2$ and NO, through the pipe, traces for OH loss and HO$_2$

220    formation could be elucidated, examples of which are shown in Figure 4. Subtraction of the two

221    OH traces in Figure 4, (upper, red trace is with NO injection and the signal corresponds to reactant

222    OH and OH produced from the titration of HO$_2$ to OH, lower, blue trace with N$_2$ injection is

223    reactant OH only) gave a resultant signal associated with HO$_2$ production in the high-pressure

224    reactor, shown the pink trace in Figure 4.  The signal from the first PMT allowed for correction of

225    the signal heights at the second PMT for changes in the probe laser power or wavelength, any

226    variations in laser power or wavelength affect the absolute signal retrieved from both PMTs;

227    however, the relative signals retrieved from the PMTs remain consistent.

228        Fits to the HO$_2$ formation traces and OH loss traces from the second cell generated kinetic

229    parameters which differed from the accurate parameters collected at the first detection axis, $k_{OH,2nd}$

230    $= (1390 \pm 44)$ s$^{-1}$ and $k_{HO2,2nd} = (1080 \pm 150)$ s$^{-1}$ where the accurate loss parameters from the first

231    cell were $k_{OH,1st} = (2389 \pm 18)$ s$^{-1}$, 2 $\sigma$ errors. This difference was the result of transport effects. By

232    comparison of the loss and formation parameters derived for OH + H$_2$O$_2$, for the first and second

233    detection cells, HO$_2$ formation rates could be assigned from a calibration plot (Figure 7).

234
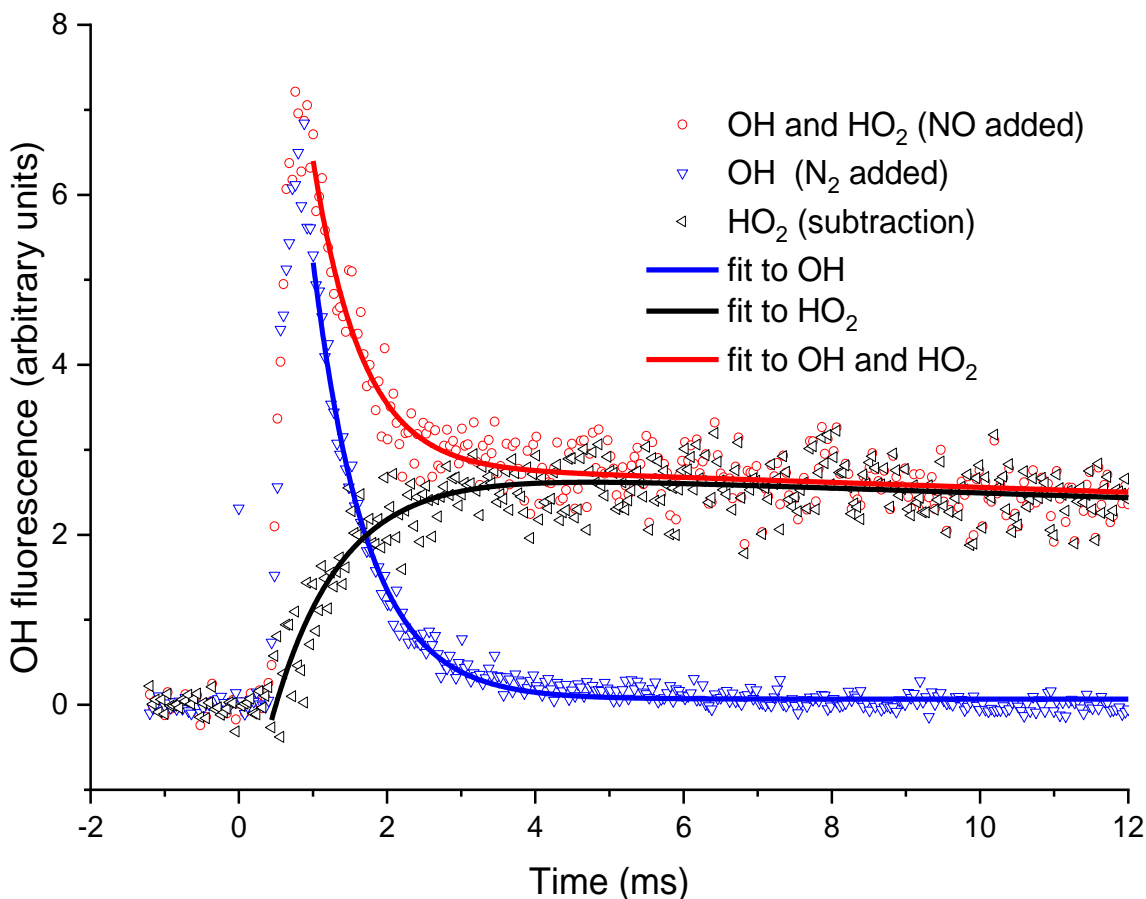
**Figure 4.** Examples of OH fluorescence traces collected at the second detection axis under the same conditions for Figure 3. The blue triangles are where $N_2$ has been injected through the pipe, i.e. no $HO_2$ to OH conversion. The OH signal profile differs from that in Figure 3, with $k_{OH,2nd}$ = $(1390 \pm 44)$ s$^{-1}$ (2 σ errors), additionally, there is a time-delay to peak OH, representing the transport time (primarily the time taken to travel from the breakdown of the jet to the second detection axis). The red circles are the OH signal obtained with NO injection. At short times the signal is dominated by reactant OH, but at times greater than 2 ms, the signal is dominated by OH titrated from the $HO_2$ product. The resultant OH trace associated with $HO_2$ formation in the high-pressure cell obtained by subtracting the two OH traces, obtained with either NO or $N_2$ injection prior to the second detection axis, shown as black triangles, a biexponential growth and decay fit, black curve, gave a formation rate coefficient, $k_{HO2,2nd}$ = $(1080 \pm 150)$ s$^{-1}$ (2 σ error).

246

Neither of the OH determinations in the two detection axes provide absolute measurements of radical concentrations. Each detection axis could be calibrated as for chamber measurements, but for our purposes a calibration reaction linking photolytically produced OH and $HO_2$ removes

250    many sources of error compared to an absolute calibration. The reaction of OH with the radical

251    precursor $H_2O_2$ which directly forms $HO_2$ with a 100 percent yield was used for calibration.

252    **OH** + $H_2O_2 \rightarrow H_2O$ + **HO$_2$**                                                         (R5)
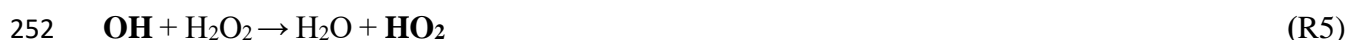
253    For reactions carried out where a reagent was added in addition to the $H_2O_2$, the resulting ratios

254    can be compared with those from the calibration reaction to allow assignment of an observed $HO_2$

255    yield. To assign the $HO_2$ yield from the test reaction required accounting for secondary $HO_2$

256    production in the high-pressure reactor, from OH + $H_2O_2$ and photolysis processes. From the

257    known rate coefficients, it was possible to calculate the fraction of OH reacting with the $H_2O_2$

258    (typically 5 – 10%) and hence the expected contribution to the $HO_2$ signal. Photolytic production

259    of $HO_2$ was accounted for by measuring the observed $HO_2$ signal in the absence of any $H_2O_2$.

260         In a typical experiment, the reaction of OH and $H_2O_2$ would be carried out four times, twice

261    in the absence of NO and twice with the addition of NO to calibrate the instrument. Exponential

262    fits to the OH decay as monitored in the first cell determine the peak OH signal. The OH signals

263    at the second detector recorded with only $N_2$ addition (reagent OH reaching the second detector)

264    and subtracted from the signal with NO added (reagent OH and $HO_2$) to give the net $HO_2$ signal.

265    This profile was fitted to, a biexponential growth and decay function, to extract the peak $HO_2$

266    signal for that set of conditions. Combinations of traces were then used to obtain an averaged value

267    (and uncertainty) of the signal on the first PMT (OH) to the net $HO_2$ signal at the second PMT for

268    this calibration reaction where OH reactant and $HO_2$ product have a 1:1 relationship. The same

269    process was then performed in the presence of the compound of study. The removal pseudo-first-

270    order rate coefficient with $H_2O_2$ and the reagent of study ($k'_{OH,1st} = k_{OH+H2O2}[H_2O_2]$ +

271    $k_{OH+TEST}[TEST]$) was compared to the removal pseudo-first-order rate coefficient with only $H_2O_2$

272    ($k'_{OH,1st} = k_{OH+H2O2}[H_2O_2]$) to assign what fraction of the OH reacted with the $H_2O_2$ precursor and

273    hence the resulting contribution to the observed $HO_2$. Comparison of the remaining peak ratio to

274    the ratio from the $H_2O_2$ and OH calibration experiment provided the experimentally derived $HO_2$

275    yield for reaction of OH and the reagent of study.

276         Branching ratios to direct $HO_2$ formation could be assigned with an accuracy of ~10 %, the

277    limitations to this were signal to noise effects, where improved signal to noise could be achieved

278    by increasing the precursor concentration and photolysis energy. However, this was limited by the

279 need to ensure pseudo-first-order conditions were maintained and to minimize radical-radical
280 processes. Ensuring the dominant reaction was between OH and the reagent of study, whilst still
281 being able to accurately measure the initial OH conditions, provided a limit to the maximum
282 removal rates achievable ($k_{OH,1st} < 30,000$ s$^{-1}$).

283

284 **3 Instrument Characterization**

285 Many reactions of atmospheric and combustion interest are studied in the presence of oxygen
286 leading to the generation of peroxy radicals ($RO_2$). For certain $RO_2$ there is a potential to generate
287 OH and $HO_2$ on a fast timescale and therefore three well known reactions were chosen to
288 characterize the instrument, OH and ethane, OH and ethylene, and OH and methanol.

289 $OH + C_2H_6 \rightarrow H_2O + C_2H_5$ (R6)

290 $OH + C_2H_4 \rightarrow HOC_2H_4$ (R7)

291 $OH + CH_3OH \rightarrow H_2O + CH_2OH, CH_2OH + O_2 \rightarrow HO_2 + HCHO$ (fast) (R8a, R9)

292 $OH + CH_3OH \rightarrow H_2O + CH_3O, CH_3O + O_2 \rightarrow HO_2 + HCHO$ (slow) (R8b, R10)
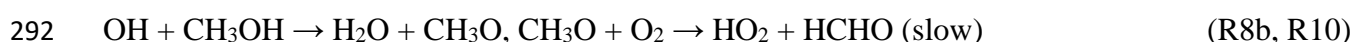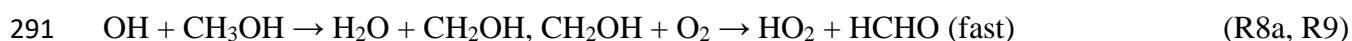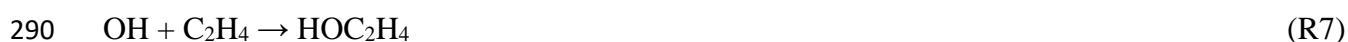
293 OH and ethane (R6) gives an assessment of any false yields generated from $RO_2$ and NO from
294 prototypical alkyl $RO_2$ species that will be formed from many atmospherically relevant reactions.
295 Ethylene and OH (R7) forms a hydroxy alkyl peroxy radical, the typical $RO_2$ species known to
296 create interferences in FAGE $HO_2$ detection systems (Fuchs et al., 2011;Hard et al., 1984;Whalley
297 et al., 2013). Minimizing and understanding the $HO_2$ yield from this reaction allowed for limits to
298 the selectivity of the instrument to be known. The reaction of OH with methanol is a well
299 understood reaction; the two isomeric radical products react with oxygen on differing timescales
300 to generate $HO_2$. Complete conversion of both isomers should yield 100 % $HO_2$.

301 As discussed in the experimental section, transport effects after the breakup of the sampling
302 jet mean that rate coefficients measured in the second cell $k_{X,2nd}$ (X = OH or $HO_2$) differ from each
303 other (transport effects scale with mass) and from those made in the first detection axis ($k_{OH,1st}$).
304 Pseudo-first-order rate coefficients from the two detection axes were compared to ascertain
305 whether measurements in the second detection axes can be used to make quantitative kinetic
306 measurements.

307         Finally, the layout of the apparatus makes it hard to accurately measure the temperature at
308 which the reaction occurs; for reactions occurring on a millisecond timescale, the relevant reaction
309 distance from the sampling pinhole is approximately 0.05 - 0.5 mm. Compared to a conventional
310 slow flow laser flash photolysis/laser induced fluorescence apparatus, where the reaction volume
311 is the overlap of the perpendicular photolysis and probe laser beams, it is hard to accurately
312 position the thermocouple and additionally, any thermocouple located close to the sampling
313 pinhole may affect the flow into the low pressure system. In addition to the difficulties in correctly
314 siting a thermocouple, there are additional errors (flow, conduction and radiative) that derive from
315 measuring the temperature of a flowing gas with a thermocouple. We have therefore performed
316 additional experiments to determine the temperature based on the well characterized and
317 temperature sensitive reaction of OH and methane.

318

319 **3.1 Interference by $RO_2$ species**

320 Selectivity in measuring $HO_2$ concentrations plays an important role in the viability of detection
321 methods for monitoring reactions important for atmospheric chemistry. At high pressures, the
322 reaction of NO with many atmospherically relevant $RO_2$ species in the presence of oxygen induces
323 $HO_2$ formation. By performing the titration in the low-pressure cell with the NO + $HO_2$ reaction
324 under 'starved NO' conditions minimized this effect. This premise was validated by measuring the
325 OH + ethane and OH + ethylene $HO_2$ yields under high oxygen conditions. In our system the
326 typical oxygen concentrations in the high pressure reactor were varied between $1 \times 10^{16}$ and $5 \times$
327 $10^{17}$ molecule $cm^{-3}$ which led to concentrations in the low pressure cell of $3 \times 10^{12}$ to $2 \times 10^{15}$
328 molecule $cm^{-3}$.

329         The reaction of OH + ethane (R6) under high oxygen conditions permits the rapid
330 formation of the ethylperoxy radical, which is an $RO_2$ radical that has a typical slow, NO
331 propagated, route to $HO_2$ formation (R11 – R12).

332 $CH_3CH_2O_2 + NO \rightarrow CH_3CH_2O + NO_2$                               (R11)
333 ($k_{11, 298 K} = 8.70 \times 10^{-12}$ $cm^3$ molecule$^{-1}$ s$^{-1}$) (Atkinson et al., 2006)

334 $CH_3CH_2O + O_2 \rightarrow CH_3CHO + HO_2$                                  (R12)
335 ($k_{12, 298 K} = 9.48 \times 10^{-15}$ $cm^3$ molecule$^{-1}$ s$^{-1}$) (Atkinson et al., 2006)

336 Under a variety of NO flows the apparent $HO_2$ yield for the $OH + C_2H_6$ system was $3 \pm 6\%$, which

337 indicates that for most reactions carried out in our system, chemical transformation by reaction

338 with NO, was sensitive to $HO_2$ rather than $RO_2$ species, where the $RO_2$ radical was the product of

339 $O_2$ addition to a simple alkyl radical.

340 The reaction of ethylene and OH (R7) in the presence of oxygen forms the

341 hydroxyethylperoxy radical ($HOCH_2CH_2O_2$), and reaction of the $HOCH_2CH_2O_2$ with NO in the

342 presence of $O_2$ provides a route for the prompt regeneration of OH. For this reaction, an apparent

343 $HO_2$ yield of $100 \pm 15\%$ was observed; however, by varying the concentration of NO added to

344 low pressure cell (between $5 \times 10^{13}$ and $5 \times 10^{14}$ molecule $cm^{-3}$), the formation rate of OH was

345 reduced minimizing the apparent yield observed ($<70\%$) and slowing the observed rate of OH

346 regeneration ($<1000$ $s^{-1}$).

347 $HOCH_2CH_2O_2 + NO \rightarrow HOCH_2CH_2O + NO_2$ (R13)
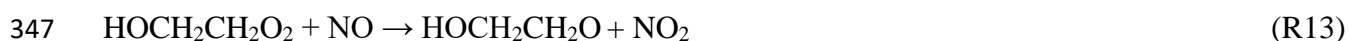
348 ($k_{13, 298 K} = 9.00 \times 10^{-12}$ $cm^3$ molecule$^{-1}$ $s^{-1}$) (Atkinson et al., 2006)

349 $HOCH_2CH_2O \rightarrow CH_2O + HOCH_2$ (R14)

350 ($k_{14, 298 K} = 1.3 \times 10^5$ $s^{-1}$) (Orlando et al., 1998)

351 $CH_2OH + O_2 \rightarrow CH_2O + HO_2$ (R9)

352 ($k_{9, 298 K} = 9.60 \times 10^{-12}$ $cm^3$ molecule$^{-1}$ $s^{-1}$) (Atkinson et al., 2006)

353 For test reagents which can generate radicals similar to hydroxyethylperoxy, our instrument will

354 detect both $HO_2$ and $RO_2$ with some selectivity to $HO_2$. Potential $RO_2$ interference can be tested

355 by examining the '$HO_2$' yield as a function of added [NO].

356

357 **3.2 OH + methanol**

358 To verify the accuracy of the method for determining $HO_2$ yields the reaction of OH and methanol

359 (R8) was examined. The branching ratio for the $\alpha$ abstraction to yield $CH_2OH$ (R8a) reported by

360 the IUPAC evaluation and based on the experimental data of McCaulley et al. (1989), is

361 $\alpha = (85 \pm 8)\%$ at room temperature with the methoxy yield as $(15 \pm 8)\%$. Reaction R8 was studied

362 at room temperature with the reaction being initiated by the photolysis of $H_2O_2$ at 248 nm. In the

363 presence of low concentrations of oxygen ($< 1 \times 10^{16}$ molecule $cm^{-3}$), the $\alpha$ abstraction still

364 leads to prompt formation of $HO_2$ via R9, but R10, $CH_3O + O_2$, occurs on a much longer timescale

365 (the ratio $k_{9,298\ K}$:$k_{10,\ 298\ K}$ is ~5000 (Atkinson et al. 2006)) and is not observed under these

366 conditions. The observed $HO_2$ yield, $(87 \pm 10)\%$ (first row of Table 1) gives the fraction of reaction

367 R8 forming $CH_2OH$ and the value is consistent with the IUPAC evaluation.

368

369 **Table 1.** $HO_2$ yields from the reaction of OH with $CH_3OH$ with varying $[O_2]$ carried out 295 K.

370 Errors given as 2 σ.

| $[O_2]$/ | HO₂ Yield (%) | | | | Average $HO_2$ |
|---|---|---|---|---|---|
| molecule cm$^{-3}$ | Expt 1 | Expt 2 | Expt 3 | Expt 4 | Yield (%) |
| $<1 \times 10^{16}$ | 90 | 89 | 79 | 88 | $(87 \pm 10)$ |
| $>2 \times 10^{18}$ | 93 | 94 | 100 | 99 | $(97 \pm 6)$ |
| $6 \times 10^{18}$ | 103 | 97 | 101 | 97 | $(99 \pm 2)$ |
| $6 \times 10^{18}$ | 98 | 102 | 98 | 98 | |

371

372 When higher concentrations of oxygen are used, the timescale for $HO_2$ production from

373 reaction R10 decreases and now both abstraction channels lead to $HO_2$ detection in our apparatus.

374 The resulting observed yield (final three rows of Table 1) is consistent with 100% conversion of

375 OH to $HO_2$ and is statistically different from the low oxygen measurements based on a Welch t-

376 test at the 98% level. The reproduction of the literature $HO_2$ yields from the reaction of OH with

377 methanol under varying $[O_2]$ demonstrates that the instrument can accurately measure $HO_2$ yields

378 with good precision. It has additionally been demonstrated that the instrument had sufficient

379 accuracy and precision to assign the branching ratios for differing abstraction channels when it

380 was possible to separate the channels by the timescale for $HO_2$ generation.

381 A possible interference that could distort the yield of $HO_2$ is the role of the radical-radical

382 reaction OH + $HO_2$ (Assaf and Fittschen, 2016):

383 $OH + HO_2 \rightarrow H_2O + O_2$      $k_{15} = 1.1 \times 10^{-10}$ cm$^3$ molecule$^{-1}$ s$^{-1}$   Atkinson et al. (2006)  (R15)
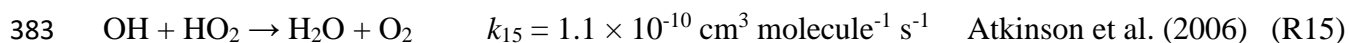
384 At the low radical concentrations used in many experiments in this work, this reaction could

385 contribute 5 – 10% of the OH loss in an OH + $H_2O_2$ calibration experiment. However, we have

386 looked at the dependence of the $HO_2$ yield from both OH/$H_2O_2$ and from OH/$CH_3OH$, but see no

387  significant effects of secondary radical-radical reaction (<5%) as the calculated $[OH]_0$ is changed

388  from $5 \times 10^{11}$ to $5 \times 10^{12}$ molecule cm$^{-3}$. For the OH/CH$_3$OH the much larger concentrations of

389  substrate used lead to faster pseudo-first order decays, so radical-radical contribution is

390  significantly reduced. The work of Assaf and Fittschen suggests that a more significant deviation

391  in the OH loss rates, and one that we ought to be to detect given the precision of our data, should

392  be observed. It is possible that our calculations of $[OH]_0$ are over-estimated, but we note that a

393  study of the OH + H$_2$O$_2$ reaction by Wine et al. (1981), where they specifically looked for the

394  interference on OH decays from R15, could find no evidence for an increase in the loss of OH,

395  when [HO$_2$] was artificially increased.

396

397  **3.3 Assessment of transport effects on observed kinetics**

398  Due to the differing conditions in the two detection regions, the kinetics observed at the first

399  detection axis, where OH LIF was performed in the jet-expanded gas, and in the second detection

400  region, where LIF is performed 15 cm downstream from the pinhole after the breakdown of the

401  jetting gas, will be treated separately. For validating the accuracy of the OH kinetics in the first

402  cell, the reactions of OH and methane (CH$_4$) (Dunlop and Tully, 1993), OH and ethylene (C$_2$H$_4$)

403  (Atkinson et al., 1982;Tully, 1983) were studied. The high accuracy and precision of this system

404  for measuring OH kinetics has further been demonstrated in a recent publication on the reaction

405  of OH and isoprene (C$_5$H$_8$) (Medeiros et al., 2018).

406  OH + CH$_4$ → H$_2$O + CH$_3$ (R16)

407  OH + C$_2$H$_4$ → HOC$_2$H$_4$ (R7)

408  OH + C$_5$H$_8$ → HOC$_5$H$_8$ (R17)

409  When these reactions were carried out at room temperature the expected bimolecular rate

410  coefficients could be reproducibly accurately measured for observed rate coefficients less than

411  150,000 s$^{-1}$.

412  Studies on the reaction of OH and ethylene at room temperature and 2.2 bar, shown in

413  Figure 5, gave a value of $k_7 = (8.33 \pm 0.16) \times 10^{-12}$ cm$^3$ molecule$^{-1}$ s$^{-1}$ (2σ errors) which matched

414  well with literature high pressure limits for OH and ethylene; where a direct pulsed laser photolysis

laser induced fluorescence study by Tully (1983) gave $k_7 = (8.47 \pm 0.24) \times 10^{-12}$ cm$^3$ molecule$^{-1}$ s$^{-1}$, and a relative rate study by Atkinson et al. (1982) found $k_7 = (8.11 \pm 0.37) \times 10^{-12}$ cm$^3$ molecule$^{-1}$ s$^{-1}$. However, for pseudo-first order rate coefficients above ~150000 s$^{-1}$, there was no longer a linear dependence of the rate coefficient with reagent concentration; transport effects are becoming significant even for OH detection in the jetting region.
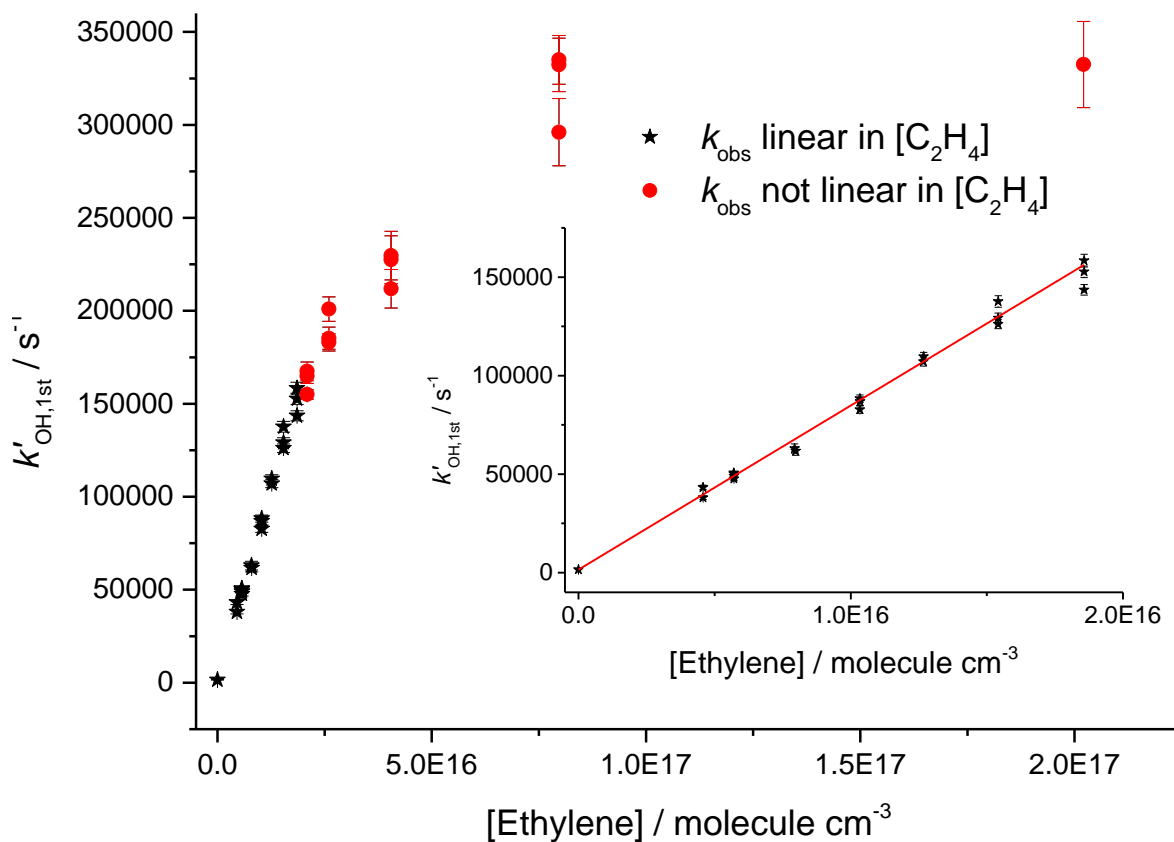
**Figure 5.** Bimolecular plot of the pseudo-first-order rate coefficient at the first detector, $k'_{OH,1st}$, vs ethylene concentration. The figure demonstrates a linear relationship below ~150,000 s$^{-1}$ (see inset for detail in linear region) but with increasing curvature, due to transport effects at higher values of $k'_{OH,1st}$. Black stars symbolize where $k'_{OH,1st}$ was linear with [C$_2$H$_4$], red circles where $k'_{OH,1st}$ showed greater than 5% deviation from linearity.

The OH traces detected in the second cell deviated from those observed from the first cell, as shown in Figures 3 and 4. There is understandably an increased time delay from time zero (the photolysis laser pulse) to arrival of OH radicals at the second detection axis due to the increased distance travelled after sampling (> 150 mm versus < 5 mm). Additionally, the arrival of OH to

431 the second axis is spread out further in time due to transport issues relating to non-linear flow

432 conditions at the breakdown of the jet, and the arrival of the OH being affected by its velocity

433 distribution (Moore and Carr, 1977;Taatjes, 2007;Baeza-Romero et al., 2012). Figure 6 shows a

434 plot of observed OH rate coefficient from the first detection axis ($k_{OH,1st}$) against observed rate

435 coefficient from the second axis ($k_{OH,2nd}$) in the reaction of OH with $H_2O_2$. For values of $k_{OH}$ below

436 2500 s$^{-1}$ it was possible to accurately assign an expected OH removal rate for reactions observed

437 in the second cell ($k_{OH,2nd}$) given the observed OH kinetics at the first detection axis ($k_{OH,1st}$). This

438 is useful to compare the kinetics of OH removal and $HO_2$ production.
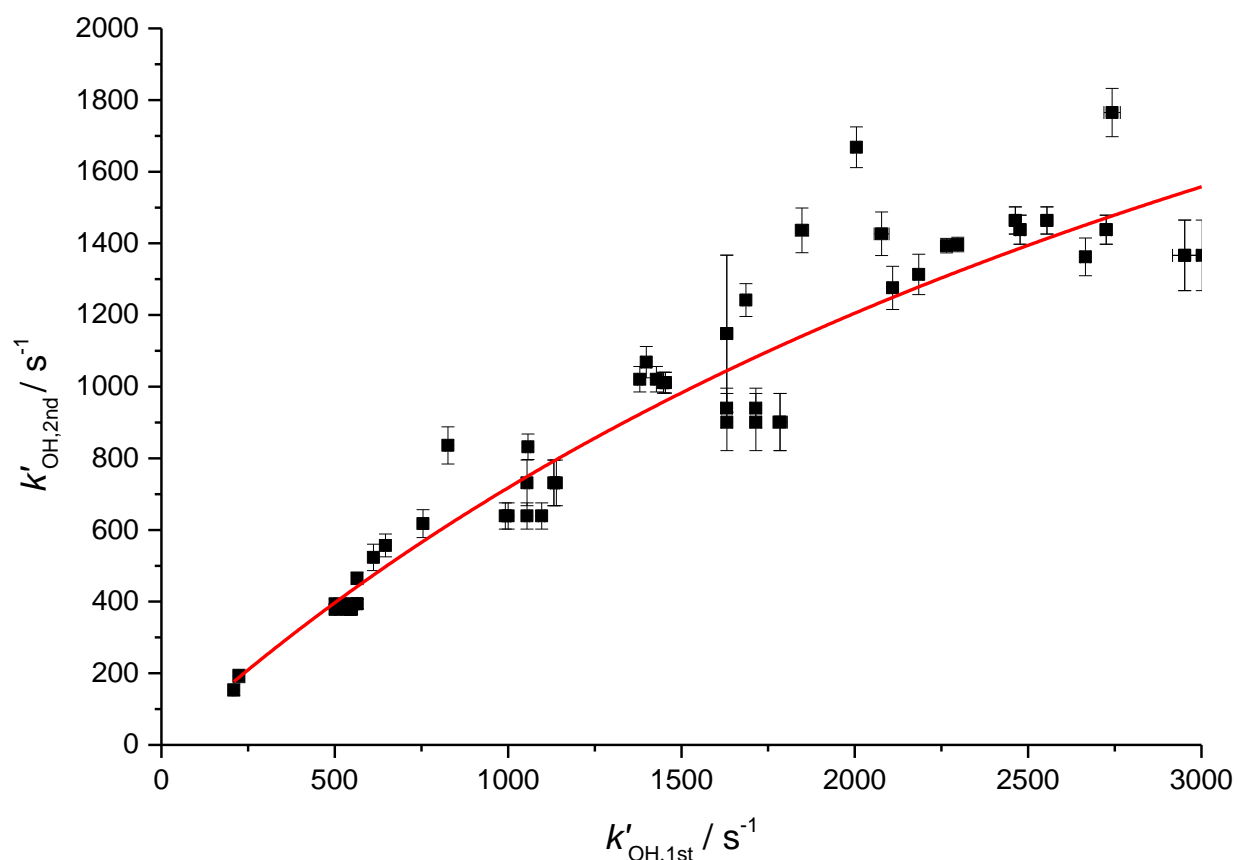
439

440 **Figure 6.** Relationship between the observed rate coefficient for the reaction of OH with $H_2O_2$

441 observed in the first cell ($k_{OH,1st}$) and the observed OH removal rate in the second cell ($k_{OH,2nd}$).

442 The difference is non-linear but a simple fit to this could be used to assign removal rates to traces

443 observed in the second cell below 2,500 s$^{-1}$. The red line is the simplified fit of the form, $y = A *$

444 $(1 - e^{-b*x})$, where A was some limit value above which no increase in measured rate coefficient

445 would be observed.

446
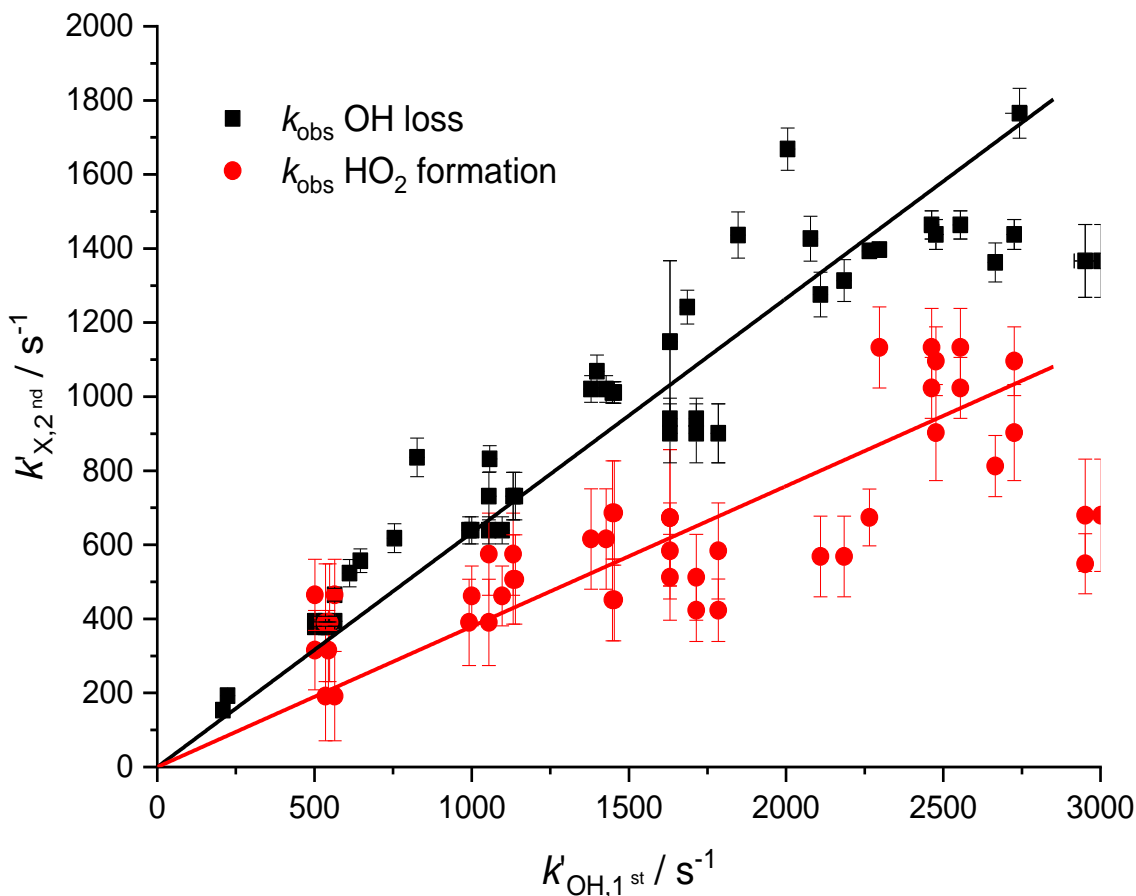
**Figure 7.** Relationship between the pseudo-first-order rate coefficient for OH loss observed in the
first cell ($k'_{OH,1st}$) from the reaction of OH with $H_2O_2$ and the observed rate coefficients measured
in the second cell ($k'_{X,2nd}$ where X = OH loss (black squares, ■) or $HO_2$ production (red circles, ●))
a non-linear fit can be used to assign removal rates and $HO_2$ formation rates to traces observed in
the second cell below 2,500 $s^{-1}$.

452

As the observed kinetics in the second cell are significantly affected by the velocity
distribution of the species being detected, there is again a deviation between the observed kinetics
expected from the measurement of the OH radicals loss and the kinetics for $HO_2$ formation due to
the differing masses of OH and $HO_2$. Figure 7 shows the pseudo-first order rate coefficients for
OH removal ($k'_{OH,2nd}$) and $HO_2$ production ($k'_{HO2,2nd}$) from the OH + $H_2O_2$ reaction determined at
the second detection axis, plotted against the OH removal at the first detection axis. The two fits
to the data shown in Figure 7 had a ratio of gradients concordant with the root of the masses for
$HO_2$ and OH, $0.60 \pm 0.14$ versus the expected relationship of 0.73. As with Figure 6, it is possible

461    to establish a calibration graph that relates the kinetics of $HO_2$ production at the second detection

462    axis with the primary kinetics taking place in the high pressure reactor. This means that the

463    timescale over which the $HO_2$ yield was observed could be assigned and therefore it is possible to

464    attribute $HO_2$ yields to fast processes, intramolecular $RO_2$ decompositions or $R + O_2$ reactions, or

465    to slower radical-radical reactions.

466

**3.4 Temperature corrections**

468    It is difficult to know the exact temperature at the pinhole as introducing a thermocouple close to

469    the region will affect the flows and cannot be used in routine operation. A translatable

470    thermocouple was passed along the axis of the high-pressure reactor over a variety of temperatures

471    and showed that the temperature of the gas at the pinhole varies with axial location. In addition,

472    radial profiles showed that in our system there was insufficient heating length to achieve uniform

473    radial heating of the laminar gas. From the axial measurements it was observed that slower flow

474    rates ($< 5$ SLM) allowed for reduced axial temperature gradients. However, these measurements

475    showed that the only manner to achieve an even thermal profile would be a static cell.

476        A permanently seated thermocouple was placed perpendicularly to the flow, close to the

477    sampling region, measurements from this thermocouple were then compared with temperature

478    assignments from the reaction of OH and methane using the temperature dependence assigned by

479    Dunlop and Tully (1993). This was performed over a range of heater settings and flows to allow

480    for temperature assignment.  This method was also applied to a standard low-pressure cell where

481    the flows can be reduced to slow enough flows that thermocouple measurements could accurately

482    define the temperature to verify the method. Additionally, the well-determined OH + ethylene

483    adduct formation equilibrium was measured over a range of temperatures to provide an additional

484    verification of the temperature assignment.

485        The method to assign a temperature from the reaction of OH and methane used the pseudo-

486    first order rate coefficients ($k'_{OH,1st}$) measured at the first detection axis over a range of added

487    methane flows. An estimate of the temperature was made from the thermocouple measurement,

488    this estimated temperature was used, along with the pressure in the reactor, to calculate the added

489    methane concentration. Comparing the predicted pseudo-first-order rate coefficient that this

490    estimated concertation provided using the literature value of $k_{OH+CH4}$ (Dunlop and Tully, 1993) to

491    the measured rate coefficient produced a difference for each point. The estimated temperature was

492    then iteratively changed to minimize the difference between estimated and measured rate

493    coefficients. For this minimum value, the difference between thermocouple measurement and

494    actual temperature was tabulated against the voltage setting for the heater. A parameterization of

495    voltage versus temperature difference was used to estimate the temperature of the reactor for

496    experiments where no OH and methane measurements were performed and has been shown to

497    reliably predict the temperature of the reactor within 7 K when measurements have been made

498    subsequently.
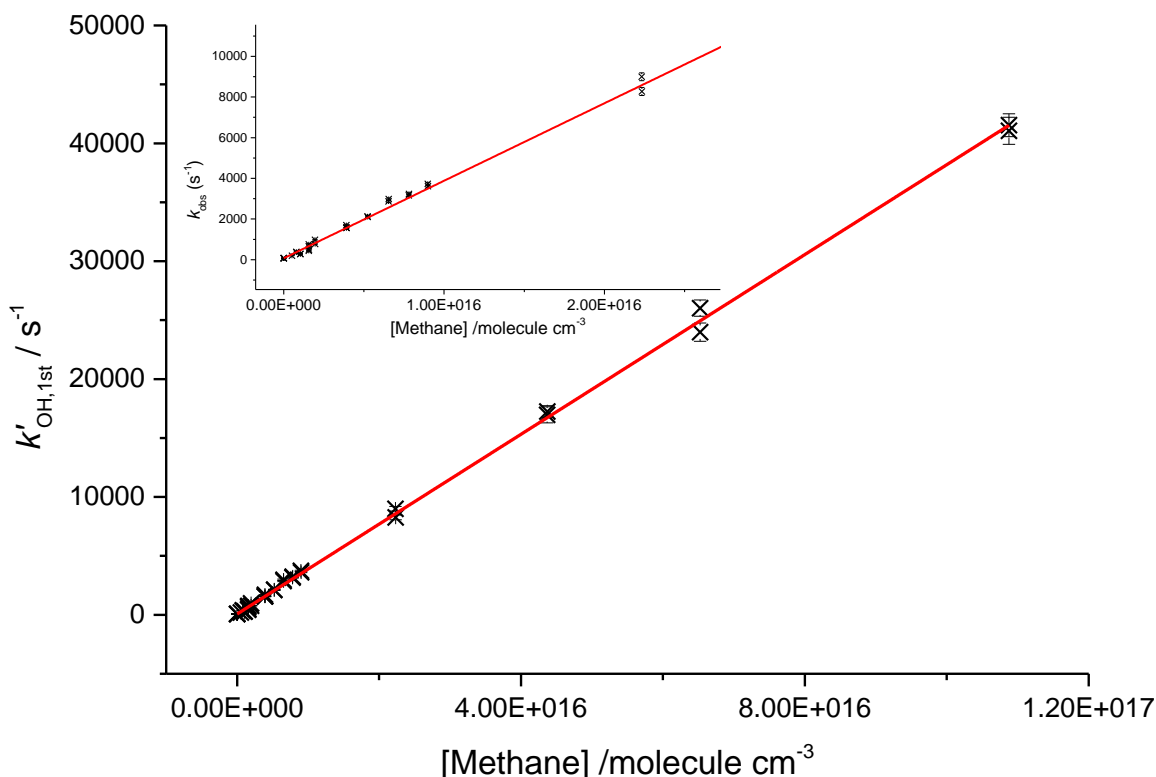
499

500    **Figure 8.** Bimolecular plot for the reaction of OH and methane at 680 K, 1760 Torr using 193 nm

501    photolysis of water as an OH precursor. Here the inset shows that even at removal rates $< 1000 \ s^{-1}$

502    the plot is still linear, indicating that within the measured experimental timescales there is little

503    deviation in temperature.

504

505       To assess the axial temperature gradients in the gas sampled through the pinhole over the

506    timescales of reactions measured, OH and methane rate coefficients were measured using

507    photolysis of water at 193 nm as a source of OH. Using water photolysis allowed for low removal

508    rates of OH by precursor and assignment of OH and methane over a range of pseudo-first-order

509    rate coefficients ($k'_{OH,1st}$) 100 – 40000 s$^{-1}$ as shown in Figure 8. This was performed at two

510    temperatures (505, 680 K), and the slope of observed OH removal rate coefficients against

511    concentration of methane appeared linear over the full range for both temperatures, thus verifying

512    that over the distances sampled within experimental timeframes there is a minimal temperature

513    gradient.

514

515    **4 Determination of Site Specific Rate Coefficients for the Reaction of OH with n-butanol**

516    The branching ratios for the sites of OH attack on n-butanol, as presented in Scheme 2, are of

517    significance to the modelling of the ignition delay times for n-butanol (Agbro et al., 2017).

518    Abstractions at the α and OH positions are chain terminating reactions at low temperatures due to

519    the formation of the relatively inert HO$_2$ radical, and abstraction at the β site leads to chain

520    propagation, through OH recycling. The new instrument permitted determination of the attack at

521    the α and β sites; attack at the α site leads to prompt HO$_2$ formation in the presence of O$_2$; at

522    elevated temperatures biexponential fits to non-single exponential OH loss traces in the absence

523    of O$_2$ (due to decomposition of the β hydroxy radical to OH and iso-butene) allowed for attack at

524    the β site to be measured.

525

526    **4.1 Room temperature OH kinetics**

527    At room temperature under pseudo-first-order conditions ([OH] $< 3 \times 10^{12}$ molecule cm$^{-3}$, [n-

528    butanol] $> 1.5 \times 10^{14}$ molecule cm$^{-3}$), the OH loss traces recovered from the first detection axis

529    from the jet expanded gas corresponded closely with single exponential decays. These decays

530    relate to the overall loss process for the reaction of OH with n-butanol:

531    OH + n-C$_4$H$_9$OH $\rightarrow$ H$_2$O + isomers of C$_4$H$_9$O        (R1)

532  The resulting rate coefficients were plotted against the concentration of butanol, in the presence of

533  both low and high oxygen, as shown in Figure 9 (low oxygen $< 5 \times 10^{15}$ molecule cm$^{-3}$, high

534  oxygen   $1.2 \times 10^{19}$ molecule cm$^{-3}$), where $k_{obs} = k_1 \times$ [butanol], giving a resultant bimolecular

535  removal rate of $k_1 = (9.24 \pm 0.40) \times 10^{-12}$ cm$^3$ molecule$^{-1}$ s$^{-1}$ under low oxygen conditions, and $k_1$

536  $= (9.23 \pm 0.15) \times 10^{-12}$ cm$^3$ molecule$^{-1}$ s$^{-1}$ under high oxygen conditions.

537
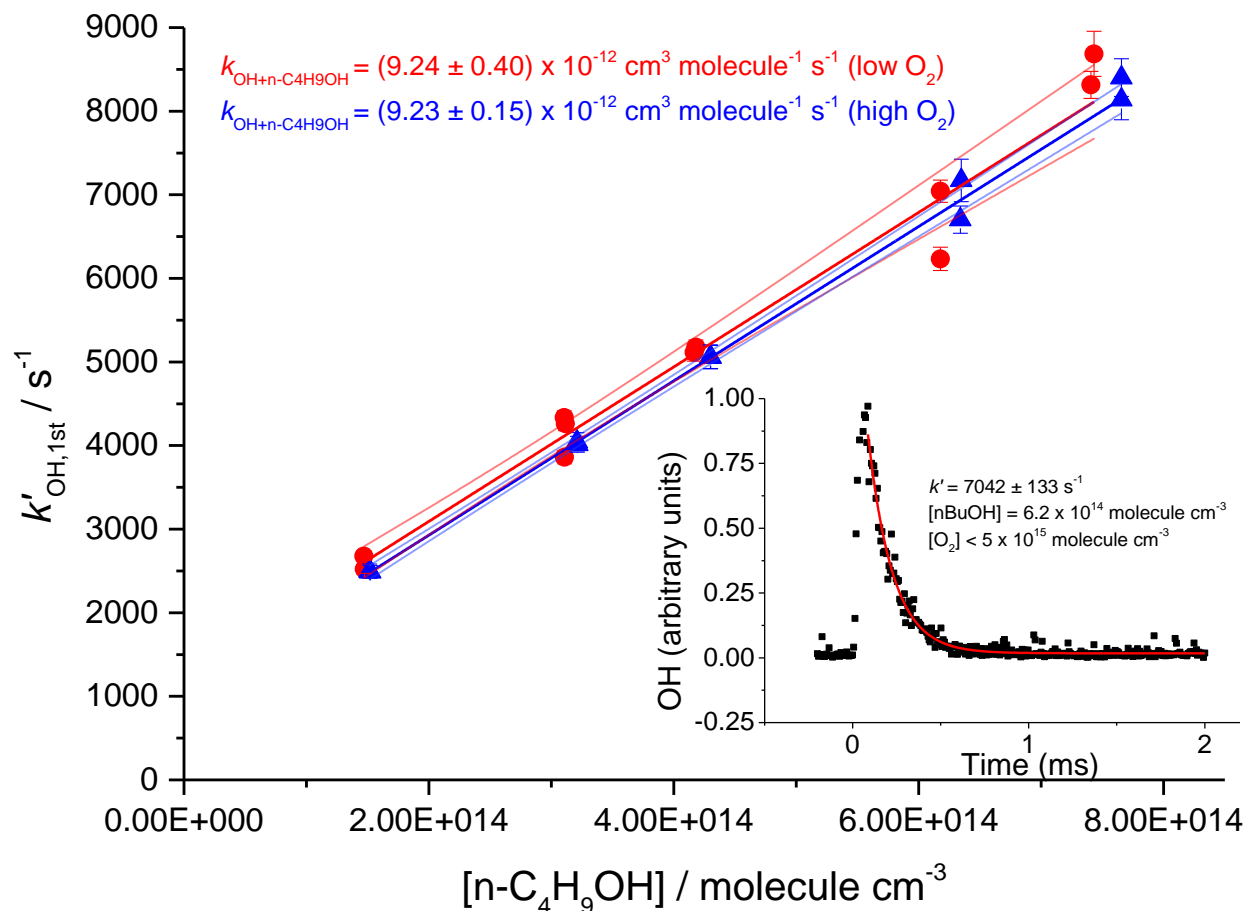
**Figure 9.** Plots $k'_{OH,1st}$ against the concentration of butanol, at two oxygen concentrations, $< 5 \times$
$10^{15}$ molecule cm$^{-3}$ and $1.2 \times 10^{19}$ molecule cm$^{-3}$. Bimolecular rate coefficients were taken from
the slopes as $(9.24 \pm 0.40) \times 10^{-12}$ cm$^3$ molecule$^{-1}$ s$^{-1}$ under low oxygen conditions (red circles with
95 % confidence limits), and $(9.23 \pm 0.15) \times 10^{-12}$ cm$^3$ molecule$^{-1}$ s$^{-1}$ under high oxygen conditions
(blue triangles with 95 % confidence limits). The inset shows a typical OH temporal profile at the
first detection axis.

544

545      The good agreement between the measured rate coefficients with varying [O$_2$] verifies that,

546  as expected under our experimental conditions at room temperature, the R radical formed from the

547  β abstraction does not undergo fragmentation to OH and but-1-ene. The resultant combined data

548  gives an overall 293 K bimolecular rate coefficient for OH and n-butanol of $k_1 = (9.24 \pm 0.21) \times$

549    $10^{-12}$ cm$^3$ molecule$^{-1}$ s$^{-1}$, which is in excellent agreement with the recent work of McGillen et al.

550    (2013) of $k_{1,296} = (9.68 \pm 0.75) \times 10^{-12}$ cm$^3$ molecule$^{-1}$ s$^{-1}$.

551

## 4.2 Room temperature HO$_2$ results

553    Experiments were carried out in high oxygen conditions ($3 \times 10^{17} - 1.2 \times 10^{18}$ molecule cm$^{-3}$), at

554    296 – 303 K, and high pressures (1800 – 2000 Torr) of N$_2$ bath gas using photolysis of hydrogen

555    peroxide at two different wavelengths (248 nm and 266 nm), and the resulting HO$_2$ yields are

556    shown in Table 2. The resulting HO$_2$ yield was determined to be ($58 \pm 7$) % at 266 nm, and ($55 \pm$

557    12) % at 248 nm. As there is no significant variation in the yield with laser wavelength or power,

558    we can treat the data in Table 2 as 12 independent estimates of the yield, giving an averaged HO$_2$

559    yield of 57% with a standard error (95%) of 6%. Therefore under the experimental conditions

560    (pressure >1800 Torr, [O$_2$] > $3 \times 10^{17}$ molecule cm$^{-3}$), the HO$_2$ yield, which originates from OH

561    attack at the α abstraction site, was ($57 \pm 6$) %, with a minor contribution from abstraction from

562    the hydroxyl group. The yield assigned is in good agreement with McGillen et al. (2013) 57%, and

563    Cavalli et al. (2002) $52 \pm 7$ %.

564

565    **Table 2.** HO$_2$ yields from experiments carried out at room temperature (293 – 298 K) with reaction

566    initiated by photolysis of H$_2$O$_2$ at 248 nm and 266 nm.

| Laser wavelength/nm | HO$_2$ Yield (%) | | | | | | | Average HO$_2$ Yield (%) |
|---|---|---|---|---|---|---|---|---|
| | Expt 1 | Expt 2 | Expt 3 | Expt 4 | Expt 5 | Expt 6 | Expt 7 | |
| 266 | $61 \pm 7$ | $54 \pm 4$ | $46 \pm 5$ | $56 \pm 7$ | $54 \pm 7$ | $67 \pm 10$ | $66 \pm 6$ | $58 \pm 7$ |
| 248 | $63 \pm 2$ | $68 \pm 2$ | $48 \pm 5$ | $52 \pm 5$ | $49 \pm 5$ | | | $55 \pm 12$ |

567

568    Experiments were carried out with photolysis at 266 nm and at a variety of laser energies at 248

569    nm, the yields remained consistent with photolysis wavelength and power. Varying the laser power

570    did alter the profiles of the HO$_2$ traces recovered; the growth rates remained unaffected but the

571    tails changed; decreasing laser power slowed the removal rate of HO$_2$ (from greater than 100 s$^{-1}$

572    to under 10 s$^{-1}$) showing that radical-radical processes are the main source of HO$_2$ loss from the

573     system. If radical-radical reactions were an important source of any observed $HO_2$ yield changing

574     laser power would have altered the $HO_2$ yield and additionally the $HO_2$ growth kinetics.

575

## 4.3 Higher temperature – $HO_2$ yield and OH recycling

577     The R radical formed from abstraction at the β site ($CH_3CH_2CHCH_2OH$) can regenerate OH and

578     form butene, Scheme 2, in the absence of added oxygen. This process was not observed at ambient

579     temperatures (293 – 305 K) but at elevated temperatures, 616 K – 657 K, the OH loss observed at

580     the first detection axis was no longer well described by a single exponential loss process, Figure

581     10. The non-exponential decays formed were due to OH being returned following decomposition

582     of the β R radical. Biexponential fits to the recycling traces gave the fraction of OH returned

583     (Medeiros et al. 2018), with an average β branching fraction of (23 ± 4)%, Table 3.

584

585     **Table 3.** OH recycling and $HO_2$ yields from experiments carried out under elevated temperatures

586     (> 600 K) all experiments were carried out with photolysis at 248 nm.

| Temperature (K) | Fraction of OH returned (%) | Observed $HO_2$ Yield (%) |
|---|---|---|
| 616 | 24.2 ± 4.1 | 54 ± 4 |
| 622 | 24.4 ± 4.9 | |
| 636 | 25.7 ± 5.6 | |
| 657 | 18.1 ± 4.0 | |

587
588
589
590

591     The $HO_2$ yield measured at an elevated temperature (616 K), where OH recycling was also

592     observed, was 54 ± 4 % (Table 3) which is within error of the value (57 ± 6 %) measured at room

593     temperature (293 K), although it is not possible to partition the $HO_2$ yield between α and OH

594     abstraction. Over the temperature range tested the branching ratio for OH attack at the α position

595     is therefore also likely to remain unchanged. With the sum of the α and β sites contributing (78 ±

596     4)%, at 616 K, the remainder of the abstraction (~22%) occurs at the δ and γ sites. These results

597     are in excellent agreement of the product study of Cavalli et al. (2002) which found (52 ± 7)% α

598     from the butanal product yield and (23 ± 4) % β from the propanal yield using FTIR detection and

599     the site specific analysis by McGillen et al. (57 % α and 26% β). The product study of Hurley et

600     al. (2009) found 44 ± 4 % α and 19 ± 2 % β values which are lower than our experimental values

601  but are within the combined error ranges. However, it should be noted that the β branching fraction

602  of 23 ± 4 % measured in this study was obtained at elevated temperatures, 616 – 657 K.

603
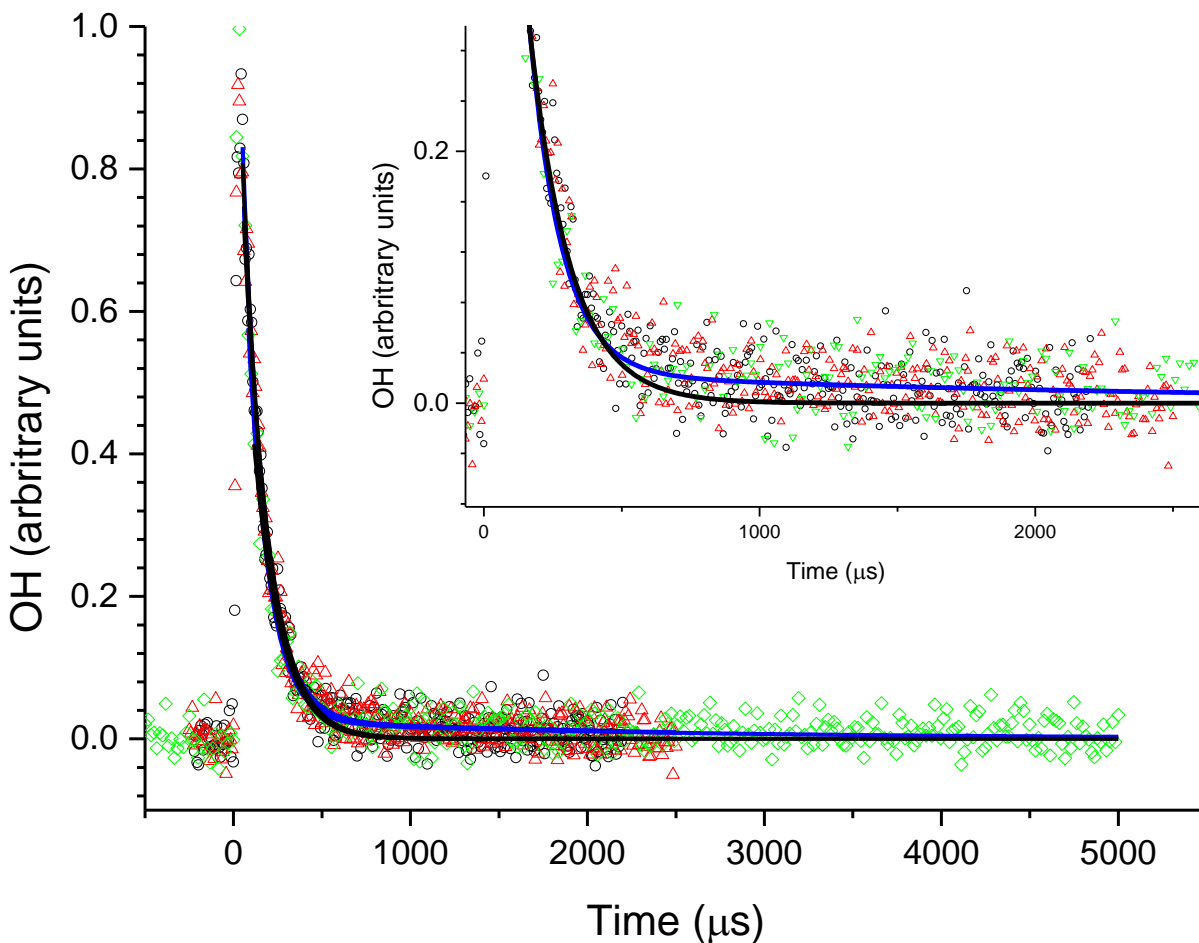
**Figure 10.** An example of the OH signal collected at the first detection axis for the reaction of OH
with n-butanol ($[nBuOH] \approx 1.4 \times 10^{15}$ molecule cm$^{-3}$, at 616 K, black, red and green points were
three consecutive decays collected with differing timescales. The black line represents the least
squares fits to an exponential decay ($k'_{1,1st} = (6780 \pm 380)$ s$^{-1}$), with the blue line representing a bi-
exponential fit ($k_{1,biexp,1st} = (8190 \pm 180)$ s$^{-1}$)). Both lines are global fits to the three experiments.

609

## 5 Summary

611  An instrument based on the FAGE technique for monitoring OH radicals and validated via

612  reproduction of the literature kinetics of several OH reactions over a wide range of temperatures

613  and pressures, has been extended to allow for simultaneous $HO_2$ and OH detection via the chemical

614  titration of $HO_2$ to OH with NO.

615  As mentioned in the introduction, the instrument has similarities to that presented by Nehr

616  et al. (2011), where a FAGE system for sequential OH and $HO_2$ is coupled to a lifetime instrument

617  and yields of $HO_2$ from OH initiated reactions are reported. Although the principles of HOx

618  detection used in both systems is similar, there are some significant differences between the two

619  instruments. Some differences relate to the reaction cell in which the kinetics takes place: 1 atm of

620  air and 298 K for Nehr et al. and 0.5 – 5 atm of any gas and 298 – 800 K for this work. However,

621  in principle, the Nehr et al. FAGE cell could be coupled to a different reaction cell to probe a wider

622  range of conditions. A more substantial difference is the timescale of the chemistry taking place.

623  Typical temporal profiles from Nehr et al. are of the order of a second compared to <10 ms in this

624  work. The enhanced sensitivity of the Nehr et al. instrument means that radical-radical reactions

625  should not interfere, but the technique may be subject to interferences from first order (or pseudo-

626  first order) reactions including heterogeneous processes.  Detection of radicals in kinetics or yield

627  experiments is difficult and studying reactions under a range of conditions is important to identify

628  systematic errors, hence both instruments have a role to play.

629  The use of $H_2O_2$ as an OH precursor has been shown to provide a reliable method of

630  internally characterizing our system for $HO_2$ yield detection. Interferences that could arise from

631  using this precursor for $HO_2$ detection have been accounted for, and the presence of water that the

632  $H_2O_2$ precursor introduces has no effect on the sensitivity of the LIF method, unlike IR absorption

633  methods.

634  It has been demonstrated that this instrument can reliably assign $HO_2$ yields and

635  simultaneously measure OH kinetics, even under conditions of high temperatures and high oxygen

636  concentrations, which could be challenging for other detection systems. Such conditions are

637  important for exploring key combustion chemistry reactions, and for converting slow

638  atmospherically relevant processes to the microsecond timescales required to minimize secondary

639  or heterogeneous chemistry.

640  By performing reactions under low NOx and low radical densities ( $<1\times10^{13}$ molecule

641  $cm^{-3}$), $HO_2$ yields formed on fast timescales ($> 300$ $s^{-1}$) can be assigned to direct $HO_2$ channels or

642  reactions of alkyl (R) radicals with oxygen. Whilst some time-resolution is lost at the $HO_2$ detector,

643 sufficient time-resolution is retained in order to separate varying sources of $HO_2$, for example the
644 two channels leading to $HO_2$ production in the $OH/CH_3OH/O_2$ system (Section 3.2) or from
645 unwanted secondary chemistry.

646       For particular reactions, illustrated in this paper by the study of OH with methanol and
647 butanol in the presence of oxygen, the simultaneous measurement of OH kinetics and $HO_2$ yields
648 can provide important site-specific information. In other systems, the onset of $HO_2$ formation could
649 allow for the assignment of new channels becoming important within complex mechanism,
650 potentially allowing for verifying the onset of OOQOOH chemistry within OH regeneration
651 processes.

652

## 6 Acknowledgements

654 A studentship from NERC through the University of Leeds 'Spheres' Doctoral Training
655 Programme for T.H. Speak is gratefully acknowledged. We are grateful to Leanne James for help
656 with some of the measurements.

657

## 7 Author Contributions

659 THS undertook most of the experimental measurements and contributed to the first draft of the
660 manuscript. DS provided input into experimental design and analysis of transport effects. MAB
661 and PWS lead the project and completed the manuscript.

662

## 8 Competing Interests

664 The authors declare that they have no conflicts of interest.

665

## 9 References

667

668 *Agbro, E., Tomlin, A. S., Lawes, M., Park, S., and Sarathy, S. M.: The influence of n-butanol blending on*
669 *the ignition delay times of gasoline and its surrogates at high pressures, Fuel, 187, 211-219,*
670 *10.1016/j.fuel.201609.052, 2017.*

671 *Assaf, E., and Fittschen, C.: Cross Section of OH Radical Overtone Transition near 7028 $cm^{-1}$ and*
672 *Measurement of the Rate Constant of the Reaction of OH with $HO_2$ Radicals, J. Phys. Chem. A, 120, 7051-*
673 *7059, 10.1021/acs.jpca.6b06477, 2016.*
674 *Assaf, E., Liu, L., Schoemaecker, C., and Fittschen, C.: Absorption spectrum and absorption cross sections*
675 *of the $2v_1$ band of $HO_2$ between 20 and 760 Torr air in the range 6636 and 6639 $cm^{-1}$, J. Quant. Spectrosc.*
676 *Radiat. Transfer, 211, 107-114, 10.1016/j.jqsrt.2018.02.035, 2018.*
677 *Atkinson, R., Aschmann, S. M., Winer, A. M., and Pitts, J. N.: Rate constants for the reaction of OH*
678 *radicals with a series of alkanes and alkenes at 299 +/- 2 K, Int. J. Chem. Kinet., 14, 507-516,*
679 *10.1002/kin.550140508, 1982.*
680 *Atkinson, R., Baulch, D. L., Cox, R. A., Crowley, J. N., Hampson, R. F., Hynes, R. G., Jenkin, M. E., Rossi, M.*
681 *J., and Troe, J.: Evaluated kinetic and photochemical data for atmospheric chemistry: Volume II - gas*
682 *phase reactions of organic species, Atmos. Chem. Phys., 6, 3625-4055, 2006.*
683 *Baeza-Romero, M. T., Blitz, M. A., Goddard, A., and Seakins, P. W.: Time-of-flight mass spectrometry for*
684 *time-resolved measurements: Some developments and applications, Int. J. Chem. Kinet., 44, 532-545,*
685 *10.1002/kin.20620, 2012.*
686 *Brune, W. H., Stevens, P. S., and Mather, J. H.: Measuring OH and $HO_2$ in the troposphere by laser-*
687 *induced fluorescence at low-pressure, J. Atmos. Sci., 52, 3328-3336, 10.1175/1520-*
688 *0469(1995)052<3328:moahit>2.0.co;2, 1995.*
689 *Cavalli, F., Geiger, H., Barnes, I., and Becker, K. H.: FTIR kinetic, product, and modeling study of the OH-*
690 *initiated oxidation of 1-butanol in air, Environmental Science & Technology, 36, 1263-1270,*
691 *10.1021/es010220s, 2002.*
692 *Crowley, J. N., Simon, F. G., Burrows, J. P., Moortgat, G. K., Jenkin, M. E., and Cox, R. A.: The $HO_2$ radical*
693 *UV absorption-spectrum measured by molecular modulation, UV diode-array spectroscopy, Journal of*
694 *Photochemistry and Photobiology A-Chemistry, 60, 1-10, 10.1016/1010-6030(91)90001-a, 1991.*
695 *Dunlop, J. R., and Tully, F. P.: A kinetic study of OH radical reactions with methane and perdeuterated*
696 *methane, J. Phys. Chem., 97, 11148-11150, 10.1021/j100145a003, 1993.*
697 *Edwards, G. D., Cantrell, C. A., Stephens, S., Hill, B., Goyea, O., Shetter, R. E., Mauldin, R. L., Kosciuch, E.,*
698 *Tanner, D. J., and Eisele, F. L.: Chemical ionization mass spectrometer instrument for the measurement of*
699 *tropospheric $HO_2$ and $RO_2$, Anal. Chem., 75, 5317-5327, 10.1021/ac034402b, 2003.*
700 *Fuchs, H., Bohn, B., Hofzumahaus, A., Holland, F., Lu, K. D., Nehr, S., Rohrer, F., and Wahner, A.:*
701 *Detection of $HO_2$ by laser-induced fluorescence: calibration and interferences from $RO_2$ radicals, Atmos.*
702 *Meas. Tech., 4, 1209-1225, 10.5194/amt-4-1209-2011, 2011.*
703 *Gianella, M., Reuter, S., Aguila, A. L., Ritchie, G. A. D., and van Helden, J. P. H.: Detection of $HO_2$ in an*
704 *atmospheric pressure plasma jet using optical feedback cavity-enhanced absorption spectroscopy, New*
705 *Journal of Physics, 18, 10.1088/1367-2630/18/11/113027, 2016.*
706 *Glowacki, D. R., Goddard, A., Hemavibool, K., Malkin, T. L., Commane, R., Anderson, F., Bloss, W. J.,*
707 *Heard, D. E., Ingham, T., Pilling, M. J., and Seakins, P. W.: Design of and initial results from a highly*
708 *instrumented reactor for atmospheric chemistry (HIRAC), Atmos. Chem. Phys., 7, 5371-5390, 2007.*
709 *Hanke, M., Uecker, J., Reiner, T., and Arnold, F.: Atmospheric peroxy radicals: ROXMAS, a new mass-*
710 *spectrometric methodology for speciated measurements of $HO_2$ and $\Sigma RO_2$ and first results, International*
711 *Journal of Mass Spectrometry, 213, 91-99, 10.1016/s1387-3806(01)00548-6, 2002.*
712 *Hard, T. M., O'Brien, R. J., Chan, C. Y., and Mehrabzadeh, A. A.: Tropospheric Free-radical determination*
713 *by FAGE, Environmental Science & Technology, 18, 768-777, 1984.*
714 *Hurley, M. D., Wallington, T. J., Lauirsen, L., Javadi, M. S., Nielsen, O. J., Yamanaka, T., and Kawasaki, M.:*
715 *Atmospheric Chemistry of n-Butanol: Kinetics, Mechanisms, and Products of Cl Atom and OH Radical*
716 *Initiated Oxidation in the Presence and Absence of NOx, J. Phys. Chem. A, 113, 7011-7020,*
717 *10.1021/jp810585c, 2009.*

718 *Jemialade, A. A., and Thrush, B. A.: Reactions of HO$_2$ with NO and NO$_2$ studied by midinfrared laser*
719 *magnetic-resonance, Journal of the Chemical Society-Faraday Transactions, 86, 3355-3363,*
720 *10.1039/ft9908603355, 1990.*
721 *McCaulley, J. A., Kelly, N., Golde, M. F., and Kaufman, F.: Kinetic studies of the reactions of F and OH with*
722 *CH$_3$OH, J. Phys. Chem., 93, 1014-1018, 10.1021/j100340a002, 1989.*
723 *McGillen, M. R., Baasandorj, M., and Burkholder, J. B.: Gas-Phase Rate Coefficients for the OH plus n-, i-,*
724 *s-, and t-Butanol Reactions Measured Between 220 and 380 K: Non-Arrhenius Behavior and Site-Specific*
725 *Reactivity, J. Phys. Chem. A, 117, 4636-4656, 10.1021/jp402702u, 2013.*
726 *Medeiros, D. J., Blitz, M. A., James, L., Speak, T. H., and Seakins, P. W.: Kinetics of the Reaction of OH with*
727 *Isoprene over a Wide Range of Temperature and Pressure Including Direct Observation of Equilibrium*
728 *with the OH Adducts, J. Phys. Chem. A, 122, 7239-7255, 10.1021/acs.jpca.8b04829, 2018.*
729 *Monks, P. S.: Gas-phase radical chemistry in the troposphere, Chemical Society Reviews, 34, 376-395,*
730 *10.1039/B307982C, 2005.*
731 *Moore, S. B., and Carr, R. W.: Molecular velocity distribution effects in kinetic studies by time-resolved*
732 *mass-spectrometry, Int. J. Mass Spectrom. Ion Processes, 24, 161-171, 10.1016/0020-7381(77)80023-5,*
733 *1977.*
734 *Nehr, S., Bohn, B., Fuchs, H., Hofzumahaus, A., and Wahner, A.: HO$_2$ formation from the OH plus benzene*
735 *reaction in the presence of O$_2$, Phys. Chem. Chem. Phys., 13, 10699-10708, 10.1039/c1cp20334g, 2011.*
736 *Onel, L., Brennan, A., Gianella, M., Ronnie, G., Aguila, A. L., Hancock, G., Whalley, L., Seakins, P. W.,*
737 *Ritchie, G. A. D., and Heard, D. E.: An intercomparison of HO$_2$ measurements by fluorescence assay by*
738 *gas expansion and cavity ring-down spectroscopy within HIRAC (Highly Instrumented Reactor for*
739 *Atmospheric Chemistry), Atmos. Meas. Tech., 10, 4877-4894, 10.5194/amt-10-4877-2017, 2017.*
740 *Orlando, J. J., Tyndall, G. S., Bilde, M., Ferronato, C., Wallington, T. J., Vereecken, L., and Peeters, J.:*
741 *Laboratory and theoretical study of the oxy radicals in the OH- and Cl-initiated oxidation of ethene, J.*
742 *Phys. Chem. A, 102, 8116-8123, 10.1021/jp981937d, 1998.*
743 *Orlando, J. J., Tyndall, G. S., and Wallington, T. J.: The atmospheric chemistry of alkoxy radicals, Chemical*
744 *Reviews, 103, 4657-4689, 2003.*
745 *Reitz, R. D., and Duraisamy, G.: Review of high efficiency and clean reactivity controlled compression*
746 *ignition (RCCI) combustion in internal combustion engines, Progress in Energy and Combustion Science,*
747 *46, 12-71, 10.1016/j.pecs.2014.05.003, 2015.*
748 *Stockwell, W. R., Lawson, C. V., Saunders, E., and Goliff, W. S.: A Review of Tropospheric Atmospheric*
749 *Chemistry and Gas-Phase Chemical Mechanisms for Air Quality Modeling, Atmosphere, 3, 1, 2012.*
750 *Stone, D., Whalley, L. K., and Heard, D. E.: Tropospheric OH and HO$_2$ radicals: field measurements and*
751 *model comparisons, Chem. Soc. Rev., 41, 6348-6404, 10.1039/c2cs35140d, 2012.*
752 *Stone, D., Blitz, M., Ingham, T., Onel, L., Medeiros, D. J., and Seakins, P. W.: An instrument to measure*
753 *fast gas phase radical kinetics at high temperatures and pressures, Review of Scientific Instruments, 87,*
754 *054102, 2016.*
755 *Taatjes, C. A., and Oh, D. B.: Time-resolved wavelength modulation spectroscopy measurements of HO$_2$*
756 *kinetics, Appl. Opt., 36, 5817-5821, 10.1364/ao.36.005817, 1997.*
757 *Taatjes, C. A.: How does the molecular velocity distribution affect kinetics measurements by time-*
758 *resolved mass spectrometry?, Int. J. Chem. Kinet., 39, 565-570, 10.1002/kin.20262, 2007.*
759 *Thiebaud, J., and Fittschen, C.: Near infrared cw-CRDS coupled to laser photolysis: Spectroscopy and*
760 *kinetics of the HO$_2$ radical, Appl. Phys. B-Lasers Opt., 85, 383-389, 10.1007/s00340-006-2304-0, 2006.*
761 *Tully, F. P.: Laser photolysis laser-induced fluorescence study of the reaction of hydroxyl radical with*
762 *ethylene, Chem. Phys. Lett., 96, 148-153, 10.1016/0009-2614(83)80481-3, 1983.*
763 *Whalley, L. K., Blitz, M. A., Desservettaz, M., Seakins, P. W., and Heard, D. E.: Reporting the sensitivity of*
764 *laser-induced fluorescence instruments used for HO$_2$ detection to an interference from RO$_2$ radicals and*

765     *introducing a novel approach that enables $HO_2$ and certain $RO_2$ types to be selectively measured, Atmos.*
766     *Meas. Tech., 6, 3425-3440, 10.5194/amt-6-3425-2013, 2013.*
767     *Wine, P. H., Semmes, D. H., and Ravishankara, A. R.: A laser flash-photolysis kinetics study of the reaction*
768     *$OH+H_2O_2 = HO_2+H_2O$, J. Chem. Phys., 75, 4390-4395, 10.1063/1.442602, 1981.*
769     *Winiberg, F. A. F., Smith, S. C., Bejan, I., Brumby, C. A., Ingham, T., Malkin, T. L., Orr, S. C., Heard, D. E.,*
770     *and Seakins, P. W.: Pressure-dependent calibration of the OH and $HO_2$ channels of a FAGE HOx*
771     *instrument using the Highly Instrumented Reactor for Atmospheric Chemistry (HIRAC), Atmos. Meas.*
772     *Tech., 8, 523-540, 10.5194/amt-8-523-2015, 2015.*
773     *Zador, J., Taatjes, C. A., and Fernandes, R. X.: Kinetics of elementary reactions in low-temperature*
774     *autoignition chemistry, Progress in Energy and Combustion Science, 37, 371-421,*
775     *10.1016/j.pecs.2010.06.006, 2011.*

776

777

778

779